Challenge Journal of STRUCTURAL MECHANICS

Vol.10 No.1 (2024)

auxetic buckling load building codes
compressive strength dynamic analysis
earthquake finite element method
girder bridge Jaya algorithm metaheuristic
algorithms modal analysis optimization
prestresing pushover analysis reinforced
concrete seismic design shallow foundations
smart concrete stability static analysis
steel structures structural dynamics
temperature effects thick plate wind

ISSN 2149-8024

TULPAR ACADEMIC PUBLISHING

Challenge Journal of Structural Mechanics

E-mail: *cjsmec@challengejournal.com*

Web page: *cjsmec.challengejournal.com*

Tulpar Academic Publishing
www.tulparpublishing.com

Challenge Journal of Structural Mechanics

CONTENTS

Research Articles

TULPAR ACADEMIC PUBLISHING

Challenge Journal of Structural Mechanics

Research Article

Strengthening of historic masonry vaults with CFRP prepreg

İsmail Hakkı Tarhan [a,*], Habib Uysal [b]

[a] *Department of Civil Engineering, Tokat Gaziosmanpaşa University, 60000 Tokat, Türkiye*
[b] *Department of Civil Engineering, Atatürk University, 25240 Erzurum, Türkiye*

ABSTRACT

Masonry vaults, frequently used in historic buildings to create large openings, have played a critical role in the survival of these buildings to the present day. These structural elements, which have been exposed to destructive effects such as earthquakes for centuries, need strengthening activities in order to transfer cultural heritage to future generations. The use of composite materials with high mechanical properties for strengthening purposes has been a popular method since the beginning of the 21st century, and its effectiveness has been proven. In this study, a masonry vault in the historical redoubts located in Erzurum, Türkiye, was modelled, and the effectiveness of various strengthening scenarios using prepreg composites was investigated. Numerical simulations were conducted with the Finite element method-based macro modelling approach. The investigation revealed that retrofitting arrangements maintained the stress distribution in masonry vaults while reducing maximum tensile stress; intrados reinforcement proved more effective, particularly the intrados-straight retrofit, with a 24% improvement, whereas extrados strengthening showed limited effectiveness.

ARTICLE INFO

Article history:
Received 14 April 2023
Revised 19 June 2023
Accepted 21 July 2023

Keywords:
Retrofit
Masonry vaults
CFRP prepreg
Numerical simulations

1. Introduction

Anatolia has been home to many civilisations from the past to the present. It is, therefore, rich in architectural works that are an important part of the cultures of these civilisations. These historical buildings, mostly constructed in the masonry building system consisting of mortar and assembled units, have been exposed to destructive effects such as earthquakes since their existence. Repair and strengthening works are vital for transferring this cultural heritage to the future. The fact that traditional strengthening methods have many disadvantages has necessitated the search for alternative methods. In parallel with technology development, using composites called fibre-reinforced polymers, obtained by combining fibres with high-strength properties with the help of epoxy resin, has become widespread in the last twenty years. In particular, composites produced by applying a pre-resin impregnation process called prepreg stand out as advanced composites. The adaptability of fibre-reinforced composites to curved geometries due to their thin and flexible nature makes it possible to use them to reinforce masonry curved structural elements.

Studies on using prepreg composites to strengthen masonry structures are limited (Cakir and Uysal 2015). Although composite materials are a proven method for retrofitting (Mahini et al. 2012; Alecci et al. 2017; Zhang et al. 2017; Hamdy et al. 2018; Tarhan and Uysal 2023), there are still critical engineering and economic issues such as application location and the amount of material to be used.

This study aims to numerically investigate the effectiveness of prepreg composites in strengthening historic masonry vaults and contributing to preserving and transferring historical structures for future generations.

2. Material and Method

2.1. Geometrical and mechanical properties of the masonry vault

To obtain the material parameter to be used in numerical simulations, the material properties of the components that make up the masonry are needed. A

* *Corresponding author*. Tel.: +90-356-252-1616 ; E-mail address: ismailhakki.tarhan@gop.edu.tr (İ. H. Tarhan)
ISSN: 2149-8024 / DOI: https://doi.org/10.20528/cjsmec.2024.01.001

masonry vault in the historical redoubts located in Aziziye, Erzurum, was monitored, and it was seen that the masonry components used in the masonry vault were Harman brick and Khorasan mortar. The material properties of the Harman brick and Khorasan mortar were taken from the literature and presented in Table 1.

The semicircular masonry barrel vault, the subject of the numerical investigation and whose sectional views are presented in Fig. 1, has a span of 100 cm, a thickness of 26 cm and a depth of 250 cm. Characteristics of the 0.125 mm thick CFRP prepreg material were taken from the manufacturer's database. The Poisson's ratio is 0.3, and Young's modulus is 1.35×10^5 MPa..

Table 1. Material properties from literature (Binici et al. 2014; Çakır and Uysal 2015).

Materials	Young's modulus (N/mm^2)	Unit volume weight (kg/m^3)	Poisson's ratio
Harman brick	2232	1650	0.2
Khorasan mortar	3200	1500	0.2

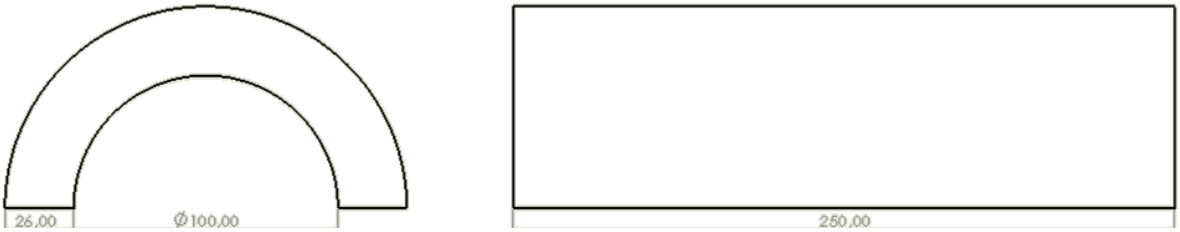

Fig. 1. Geometrical properties of the masonry vault.

2.2. Numerical modelling

The numerical modelling of masonry is a complex problem due to the heterogeneous nature of masonry. The modelling methods are based on three approaches (Fig. 2). These approaches are micro modelling, simplified micro modelling and macro modelling. Although more accurate and detailed solutions can be obtained with the micro-modelling approach in which masonry units and mortar are modelled separately, it is preferred for solving small-sized problems due to the computational burden required. On the other hand, the macro modelling approach, which considers masonry as a single composite material, provides fast and highly accurate results about the global behaviour of the structure or structural element. Macro modelling is a popular method due to the low computational load and result file storage requirements (Lourenço et al. 1996).

In this study, the macro modelling method was adopted, assuming that the masonry shows isotropic and linear elastic behaviour as Tarhan and Uysal (2023) followed.

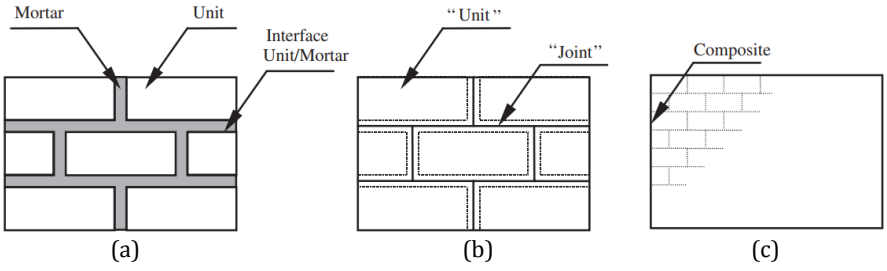

Fig. 2. Modelling methods for masonry structures:
(a) Detailed micro-modelling; (b) Simplified micro-modelling; (c) Macro-modelling.

The Young's modulus of the homogeneous material consisting of a combination of unit and mortar was calculated using Eq. (1) proposed by Lourenço et al. (2002).

$$E_a = \frac{t_m + t_b}{\frac{t_m}{E_m} + \frac{t_b}{E_b}} \quad (1)$$

where t_m, t_b, E_m and E_b represent the thickness and Young's modulus for mortar and brick, respectively, and E_a represents Young's modulus of the new composite material. According to the formulation, Young's modulus of the new material was calculated as 2560.5 MPa and defined in the numerical model. The material properties adopted for the numerical model are presented in Table 2. Details can be found in Tarhan (2018).

Solidworks and ANSYS Workbench programs were used to create and analyse the models. The numerical model was divided into finite elements with a size of approximately 50 mm (Fig. 3). The numerical model, fixed to the ground at both feet, was statically analysed under gravity. A 40 N/mm load was applied from the middle of the spanning through its depth in addition to gravity load.

Table 2. Material parameters used in modelling.

Materials	Young's modulus (N/mm^2)	Unit volume weight (kg/m^3)	Poisson's ratio
Masonry	2560.5	1543.7	0.2
CFRP Prepreg	135000	1600	0.3

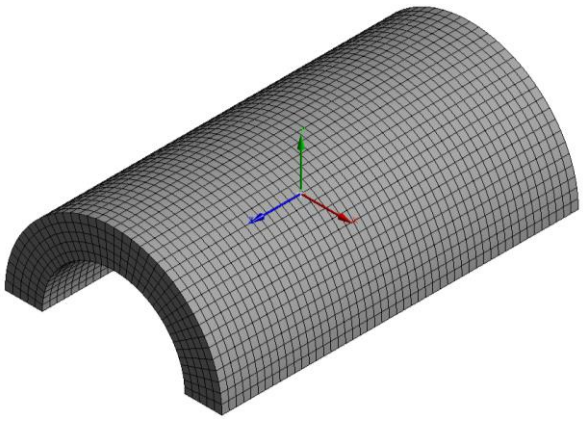

Fig. 3. View of the model divided into finite elements in 50 mm size.

Four different composite layouts were determined as reinforcement arrangements considering the inner and outer surfaces of the vault separately. For the reinforcement arrangements, 15 cm wide strips were used. Depending on the path followed by the composite, these arrangements were considered in two categories: straight and curved. The straight composite arrangement represents the case where the placement of CFRP prepreg material follows a straight line along the vault depth. The curved category refers to the composite placement along the curved path of the vault. In the straight reinforcement arrangement, the composites were applied in five pieces from the intrados of the vault and along a depth of 2.5 m. The composite strips were applied at 20 cm intervals in the case of intrados reinforcement, while the intervals were 40 cm in the case of extrados strengthening. In the curved reinforcement arrangement, eight pieces of composite strips were placed at 18.5 cm intervals along the depth of the vault. The volume of material used in all arrangements is approximately equal. For more information, see Tarhan (2018). The view of the reinforcement type is given in Fig. 4.

In order to clarify the comparison of retrofitting arrangements and the conclusions, a simple formulation named the percentage of effectiveness (PE) was used, presented in Eq. (2), where the change in maximum tensile stress is expressed as a percentage.

$$PE = \frac{|\sigma_i - \sigma_{ii}|}{\sigma_i} \times 100 \tag{2}$$

Here, σ_i represents the maximum tensile stress in the reference, i.e., the unreinforced vault model, and σ_{ii} represents the maximum tensile stress in the model reinforced with the retrofitting arrangement for which the effectiveness percentage is calculated..

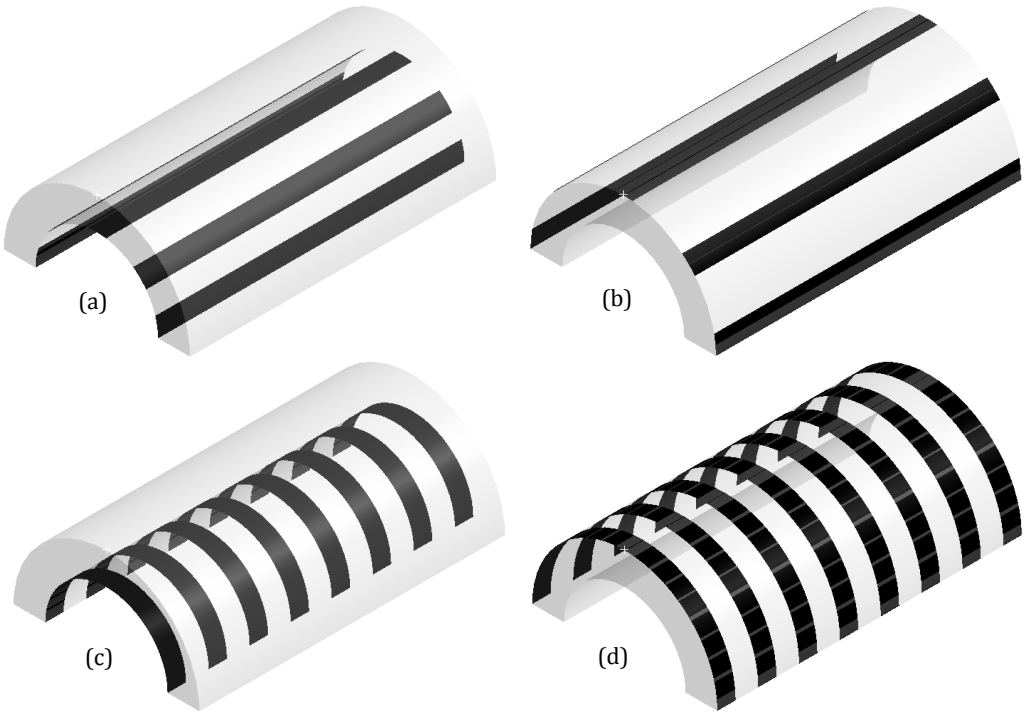

Fig. 4. Reinforcement arrangements:
a) Intrados-straight layout; b) Extrados-straight layout; c) Intrados-curved layout; d) Extrados-curved layout.

Table 3. The number of elements and nodes depending on the strengthening type.

Strengthening arrangement	Number of elements	Number of nodes
Unstrengthened (Reference)	9000	42873
Intrados - straight	10250	46227
Extrados - straight	10250	46227
Intrados - curved	10662	47622
Extrados - curved	10662	47622

3. Results and Discussion

In this section, the numerical analysis results of the proposed retrofitting arrangements are evaluated regarding maximum principal stress, referencing the results of the unreinforced masonry vault model.

Unreinforced masonry vault analysis results are presented in Fig. 5. The distribution of tensile stresses occurred parallel to the classical five hinge formation region in the intrados part of the vault crown region, the vault back, and the support region intrados of the vault. It was determined that the maximum tensile stress of 0.34 MPa occurred in the vault crown region and the intrados part. In the stress distribution, some tensile stress accumulation was observed adjacent to the applied line loading. Since this distribution is due to the type of load application, it is not a location where tensile stress is expected to occur and was ignored in the evaluation.

The tensile stress distribution of the masonry vault reinforced with the intrados-straight reinforcement arrangement is presented in Fig. 6. The distribution of tensile stress did not change in general, and the maximum tensile stress value was found to be 0.26 MPa. PE was determined as 24%.

The results of the analysis of the reinforced model with the arrangement in which the composite layout is applied from extrados and straight are presented in Fig. 7. Maximum principal stress distribution has the same distribution as the reference. The maximum tensile stress value is 0.33 MPa and has the same distribution. The PE of this strengthening arrangement is 3%.

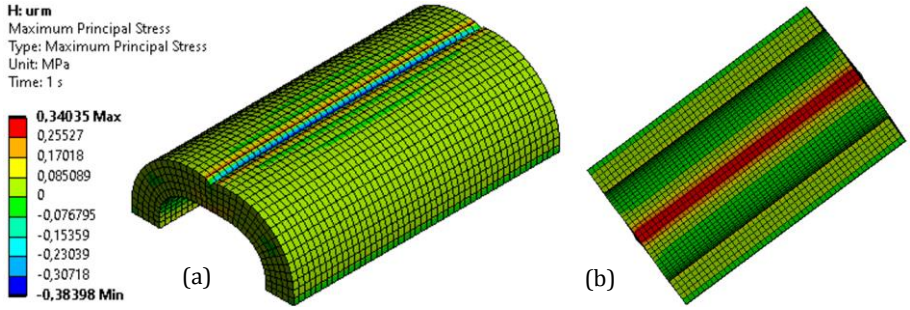

Fig. 5. Maximum principal stress distribution of unstrengthened model: a) Isometric view; b) Bottom view.

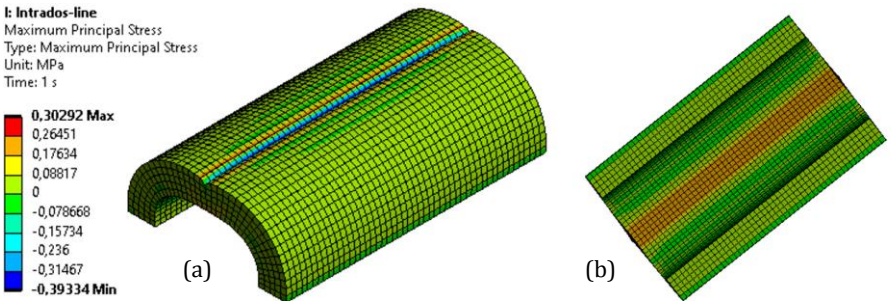

Fig. 6. Maximum principal stress distribution (intrados-straight reinforcement): a) Isometric view; b) Bottom view.

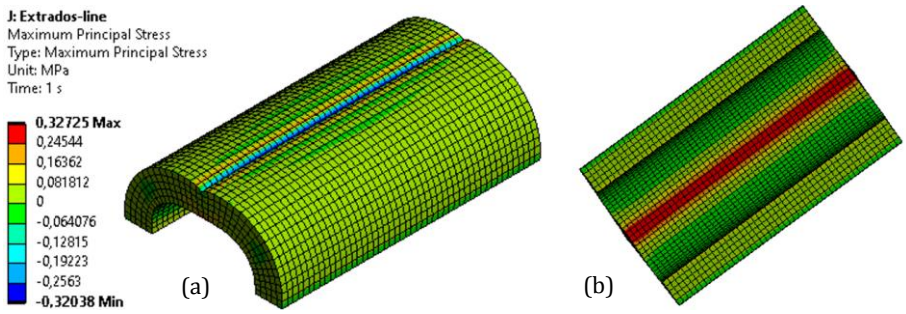

Fig. 7. Maximum principal stress distribution (extrados-straight reinforcement): a) Isometric view; b) Bottom view.

The maximum tensile stress was determined as 0.31 MPa in the intrados-curved arrangement with 9% PE, whose stress distribution is presented in Fig. 8. In addition, the stress distribution varies in a wide range in the region where the maximum tensile stress occurs. Accordingly, as shown in Fig. 8, the stress distribution in the area where the maximum stress occurs is not uniform, unlike the others.

The stress distribution of the reinforced model with the composite arrangement on the extrados and along the curved path is presented in Fig. 9. The maximum tensile stress value was almost the same as the reference value, and a PE of 0.8% was obtained.

The maximum tensile stress values of the models and the effectiveness percentages obtained from the models are presented in Fig. 10, together with the reinforcement category and location information. As stated by Valluzzi et al. (2001) and Foraboschi (2004), all of the models reinforced with composite increased the load-carrying capacity. Foraboschi (2004), Oliveira et al. (2010) and Tarhan and Uysal (2023) reported that intrados strengthening is more effective, as found in this study. The most effective reinforcement arrangement was identified as intrados-straight. Moreover, straight reinforcement was more effective than the curved one of the arrangements with the same location. On the other hand, the extrados strengthening arrangement was insufficient to limit the tensile stresses in the reference model.

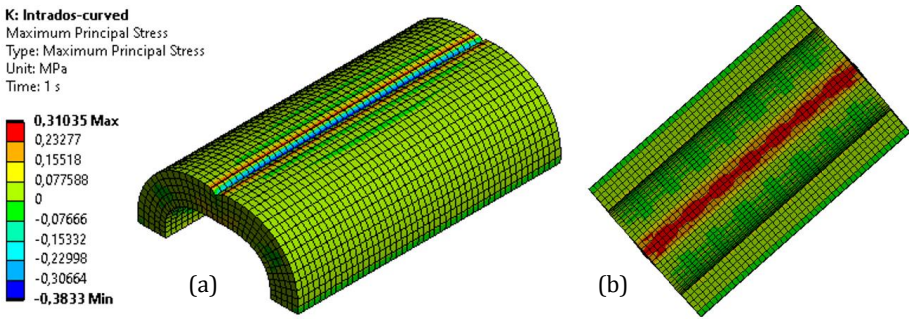

Fig. 8. Maximum principal stress distribution (intrados-curved reinforcement): a) Isometric view; b) Bottom view.

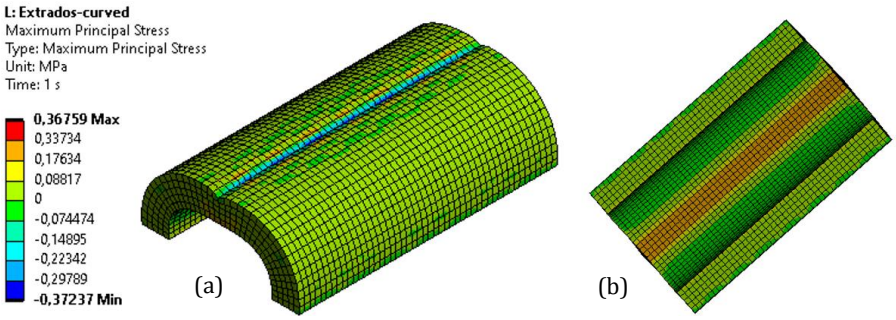

Fig. 9. Maximum principal stress distribution (extrados-curved reinforcement): a) Isometric view; b) Bottom view.

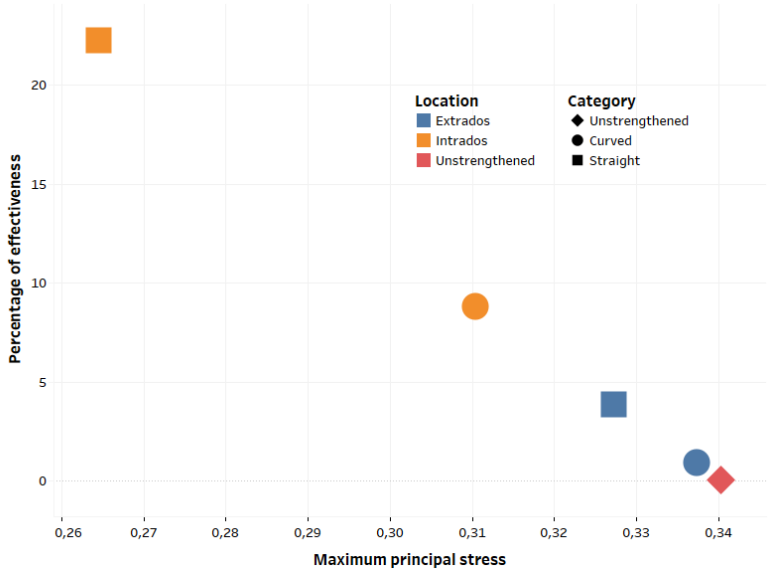

Fig. 10. Effectiveness of models regarding restricting maximum principal stress.

4. Conclusions

The current study investigated four composite layouts to strengthen a historical masonry vault in Erzurum province. The models were compared in terms of maximum principal stress, i.e., tensile stress, and their effectiveness was evaluated.

According to the results of the investigation of the linear behaviour of masonry vaults, the retrofitting arrangements did not change the distribution of tensile stresses but limited the maximum tensile stress amount.

Intrados reinforcement arrangements are more effective than extrados. In addition, the intrados-straight retrofit arrangement is the most effective, with a *PE* of 24%. On the other hand, extrados strengthening arrangements showed very low effectiveness. With this study's results, where the masonry's linear behaviour is taken as a reference, data parallel to the literature have been obtained. On this basis, the effectiveness of various reinforcement arrangements has been investigated, and recommendations have been given. Further research, such as the determination of composite placement, efficacy of different materials and nonlinear behaviour of reinforced models, are important aspects of the subject that must be addressed.

Determining the optimum composite placement by revealing their effectiveness experimentally is further research suggests that will significantly contribute to the literature.

A study comparing composite materials and determining the most effective material can contribute to the literature. While making this comparison, it may be critical for strengthening recommendations that the results are presented with experimental and non-linear analyses, taking into account that the bond that different materials will form with masonry may be different. On the other hand, it is foreseen that a well-structured formulation is needed to determine the amount of material to be used to make a fair comparison of composite materials with different thicknesses, fibre ratios and stiffness.

Acknowledgements

None declared.

Funding

The authors received no financial support for the research, authorship, and/or publication of this manuscript.

Conflict of Interest

The authors declared no potential conflicts of interest with respect to the research, authorship, and/or publication of this manuscript.

Author Contributions

All of the authors made substantial contributions to conception and design, or acquisition of data, or analysis and interpretation of data; were involved in drafting the manuscript or revising it critically for important intellectual content; and gave final approval of the version to be published.

Data Availability

The datasets created and/or analyzed during the current study are not publicly available, but are available from the corresponding author upon reasonable request.

REFERENCES

Alecci V, De Stefano M, Focacci F, Luciano R, Rovero L, Stipo G (2017). Strengthening masonry arches with lime-based mortar composite. *Buildings*, 7(2), 49.

Binici B, Canbay E, Yakut A, Aldemir A, Çobanoğlu B (2014). Risk Değerlendirmesi için Gerçek Yığma Yapılar Üzerinde Sismik Deneyler. https://eski.imo.org.tr/resimler/dosya_ekler/2bee01c3f5f96ab_ek.pdf?tipi=2&turu=X&sube=16 [accessed 13-04-2023]. (in Turkish)

Cakir F, Uysal H (2015). Experimental modal analysis of brick masonry arches strengthened prepreg composites. *Journal of Cultural Heritage*, 16(3), 284-292.

Foraboschi P (2004). Strengthening of masonry arches with fiber-reinforced polymer strips. *Journal of Composites for Construction*, 8(3), 191-202.

Hamdy G, Kamal O, Al-Hariri O, El-Salakawy T (2018). Plane and vaulted masonry elements strengthened by different techniques–Testing, numerical modeling and nonlinear analysis. *Journal of Building Engineering*, 15, 203-217.

Lourenço PB (1996). A user/programmer guide for the micro-modeling of masonry structures. *Report*, 3(1.31), 35.

Lourenço PB (2002). Computations on historic masonry structures. *Progress in Structural Engineering and Materials*. 4(3), 301-319.

Mahini SS, Eslami A, Ronagh HR (2012). Lateral performance and load carrying capacity of an unreinforced, CFRP-retrofitted historical masonry vault–A case study. *Construction and Building Materials*, 28(1), 146-156.

Oliveira DV, Basilio I, Lourenço PB (2010). Experimental behavior of FRP strengthened masonry arches. *Journal of Composites for Construction*, 14(3), 312-322.

Tarhan İH (2018). Investigation by Finite Element Method of Masonry Vaults that Reinforced with Composites. *M.Sc. thesis*, Atatürk University, Erzurum, Türkiye.

Tarhan İH, Uysal H (2023). Topology optimization of the FRP for strengthening of masonry barrel vaults. *Engineering Failure Analysis*, 107390.

Valluzzi MR, Valdemarca M, Modena C (2001). Behavior of brick masonry vaults strengthened by FRP laminates. *Journal of Composites for Construction*, 5(3), 163-169.

Zhang S, Yang D, Sheng Y, Garrity SW, Xu L (2017). Numerical modelling of FRP-reinforced masonry walls under in-plane seismic loading. *Construction and Building Materials*, 134, 649-663.

Challenge Journal of Structural Mechanics

Research Article

Effect of soil types on nonlinear earthquake behavior of buildings

Memduh Karalar [a,*], Murat Demirköse [a], Necati Mert [b]

[a] *Department of Civil Engineering, Zonguldak Bülent Ecevit University, 67100 Zonguldak, Türkiye*
[b] *Department of Civil Engineering, Sakarya University, 54050 Sakarya, Türkiye*

ABSTRACT

The Winkler method, which is widely used today, assumes that the soil behaves elastically and does not take into account the soil shear stress values, it is insufficient to reflect the actual soil behavior. Especially in the earthquake calculations of rigid and massive structures such as high-rise buildings, dams, suspension bridges, viaducts, it is necessary to consider soil as a dynamic system that changes shape and affects the behavior of the structure in terms of inertia. In response to the effect of soil on the structure, the structure also affects soil both kinematically and dynamically. Thus, in the absence of the structure, the earthquake data, which is only a result of the dynamic behavior of the soil in its internal structure, now acquires a more complex soil motion characteristic that is also affected by the presence of the structure. The observations made in some earthquakes show that the changes between the records taken simultaneously on the building foundation and at soil surface not a point far from foundation, show that the structure also affects soil therefore soil motion in response to the effect of the earthquake on the structure. In this study, the effect of soil types on the nonlinear seismic behavior of reinforced concrete structures was investigated. For this purpose, 7-storey building models with different plans and rigidities were created. The behavior of these models under 11 different earthquake loads for the ZA, ZB, ZC, ZD, ZE soil types specified in the Turkish Building Earthquake Code has been investigated. Analyzes were made using the time history method with the help of the SAP2000 program. As a result of the analysis, the displacements, plastic hinge formation, Effective inter-storey drift and period values obtained for different models were compared.

ARTICLE INFO

Article history:
Received 20 June 2023
Revised 21 July 2023
Accepted 4 August 2023

Keywords:
Soil-structure interaction
Time history method
3D dynamic analysis
Soil dominant period

1. Introduction

Since the earthquake effect is a vibrational movement in the earth's crust, it creates a dynamic influence by creating a time-dependent displacement movement on the supports of the buildings. In most of the structural analysis, the foundations are considered as built-in and it is assumed that there is no displacement or rotation in the foundations. However, in reality, collapses and rotations occur in the foundations. In the case of a dynamic loading such as an earthquake acting on the structures, the structure and soil move together and affect each other's behavior (Aydınoglu 1977; Aydınoğlu 1981). According to the stiffness of soil, the behavior of the structures on different soil layers under the influence of earthquakes constitutes a large part of the structure-soil interaction problem. In this case, the structure-soil interaction must be taken into account. In earthquake calculations of such structures, soil environment should be considered as a dynamic system that changes shape and affects the behavior of the structure in terms of inertia (Aydınoglu 1994; Lysmer et al. 1969). In response to the influence of soil on the structure, the structure also affects soil both kinematically and dynamically. In cases where the structure does not exist, the earthquake data, which is only a result of the dynamic behavior of the soil itself, turns into a more complex ground motion as a result of the presence of the structure. Records taken during earthquakes

* *Corresponding author*. Tel.: +90-372-291-2118 ; E-mail address: memduhkaralar@beun.edu.tr (M. Karalar)
ISSN: 2149-8024 / DOI: https://doi.org/10.20528/cjsmec.2024.01.002

have shown that the results obtained from soil with a structure and the soil without any structure in the same region is different (Bettes and Zienkiewicz 1969; Parmelee 1967). These differences prove that ın response to the influence of soil on the structure, the structure also affects soil and therefore the earthquake record. Lysmer and Kuhmeyer (1969) developed an artificial boundary model, which it was called viscous boundary conditions, and in the dynamic analysis of the structure-soil system, they prevented the reflection of some of the waves scattered from the source by hitting the artificial boundaries. In another study, Bettess and Zienkiewicz (1969) established the Infinite Element Model for static and harmonic loads. This method was used by Medina (1980) for modeling the soil structure dynamic interaction. In later studies, Iida (1998) conducted a 3-D non-linear, structure-ground dynamic interaction analysis using the finite element technique, by considering the buildings of different storey heights, to investigate the cause of heavy damage especially to medium-height buildings in the Lakebed region with the 1985 Mexico City earthquake. In these analyzes, structures were examined in different categories for linear and non-linear situations, taking into account both fixed-support and structure-soil interaction. As a result, it was observed that the situations where the interaction was not taken into account were insufficient to explain the causes of damage in the buildings. Another investigation was performed by Avilés and Pérez-Rocha (1998). In this investigation, Avilés and Pérez-Rocha (1998) examined the influences of foundation embedment depth on the behavior of the building soil system, the dominant period and damping of the building under dynamic loads. At the end of this investigation, the numerical solution was evaluated on a system consisting of a single-storey structure embedded in a homogeneous, elastic semi-infinite ground. Gouasmia and Djeghaba (2007) also investigated the influences of a multi-storey building on the earthquake influence due to different soil properties and local soil thicknesses, taking into account the structure-soil dynamic interaction. As a result of this study, analyzes were made using soil properties and local soil thickness as variables, and from the findings, it was noted that in case of loose soil with low shear wave velocity and with the increase in soil layer depth, the response of the structure increased and the natural periods were prolonged. The other investigation was performed by Ichihara et al. (2021). In this study, Ichihara et al. (2021) estimated correctly the influence of the nonlinear behavior of the soil-structure interface on the response of the reactor structure with a 3-D finite element model. At the end of this investigation, it was measured that soil separation and sliding have an excessive influence on the spreading features of the soil pressure along sidewalls and max. acceleration response. Bolisetti et al. (2018) offered a valuation of the industry-standard soil-structure interaction analysis codes, SASSI and LS-DYNA for linear and nonlinear SSI analyses of safety-related nuclear constructions and commercial constructions. At the end of this investigation, it was observed that nonlinear soil-structure interaction calculations might be considerably different from those made using linear frequency-domain codes. The other study was performed by Chian et al. (2019). In this study, the performance of structures and geotechnical constructions within the affected areas were examined to improvement visions on their design and construction deficiencies. Chian et al. (2019) contained building damages recognized to a combination of structural resonance, deficiencies in reinforcement detailing, vulnerability to soft story failure, ground settlement, soil liquefaction, and landslides. It was established that constructions which were strictly damaged had natural construction frequencies corresponding with the dominant frequencies of the ground shaking. In another investigation, Vicencio and Alexander (2018) estimated the influence of Soil-Structure Interaction among two structures assumed altered constraints of the structures, inter-building spacing, and soil type. At the end of this investigation, the consequences presented that there were both unfavorable and useful arrangements of the two structures that create significant changes among nonlinear structure-soil-structure interaction and non-linear soil-structure interaction. Essentially it was proved that the opposing influences of structure-soil-structure interaction might be more marked while the nonlinear soil behaviour was supposed. Oz et al. (2020) examined and compared the influence of soil-structure interaction on the seismic ability and response calculations of existing structures built on the several soil conditions altering from stiff to soft. Furthermore, nonlinear static pushover analyses were performed to detect the influence of soil-structure interaction on the capability curvatures of designated structures and the consequences were compared. Other investigations were also performed in the literature (Castelli et al. 2021). At the end of this study; it was detected that the interaction among soil and the construction changes the total displacement ability of constructions in preference to increasing it. As detected from these studies in the literature; there are few investigations about the nonlinear seismic behavior of buildings. Moreover, according to seismic design codes, the effect of soil properties on the nonlinear seismic behavior of buildings has not been observed in the past in detail. For that reason, one of the most significant aims of this study is to determine the influence of soil properties on the nonlinear seismic behavior of buildings. For this purpose, 7-storey building models with different plans and rigidities were created. Then, the behavior of these models under 11 earthquake loads for the different soil types specified in the Turkish Building Earthquake Code 2018 was examined. Analyzes were made using the Non-Linear Analysis Method in the Time History with the help of the SAP2000 program. As a result of the analysis, displacements, plastic hinge formation, max. inter story drift ratio and period values obtained for different models were compared. As a result, this research study is very important to fill these absences in the literature.

2. Scope of the Study

The aim of this study is to examine the building-soil interaction from different perspectives by giving information about the previous literature studies on building-

ground interaction. Furthermore, to investigate the influence of non-linear seismic behavior of buildings on soil types in the context of structure-soil interaction. Since the Winkler method, which is widely used today, accepts the soil as elastic and does not take into account the shear stress values for the real soil, it is insufficient to reflect the actual soil behavior. Therefore, to model the ground more realistically, the ground was first divided into small pieces using the finite element method, which was modeled as solid in the SAP2000 package program. Each part has 8 corners and 6 types of springs were assigned to this corner as horizontal translation and angular rotation in the x, y, z direction, and the numerical values of these springs were found with the formulas developed by Gazetas (1991). Viscous boundaries are defined on the edges of the modeled soils. For this, frame system 7-storey building is defined in SAP2000. Details are given in the following subsections.

2.1. Features of structure soil model

The Direct Method was used to examine the influence of soil types on the non-linear seismic behavior of buildings. In the direct analysis method, the cutting surfaces must be chosen at a very far distance from the structure in order to obtain realistic results. However, the finite element region does not need to be very large for the model to be solvable. When the ground region bounded by the cut-off boundaries is modeled with SEM, the waves propagating in the closed environment collide with the boundaries and return to the analysis environment and adversely affect the solution.

In order to prevent this situation, the cut-off boundaries should be arranged in such a way as to provide wave permeability with special boundary conditions as shown in Fig. 1 (Guiterrez and Chopra 1978). Viscous boundaries are defined for the cutting surfaces depending on the effective damping and stiffness of soil.

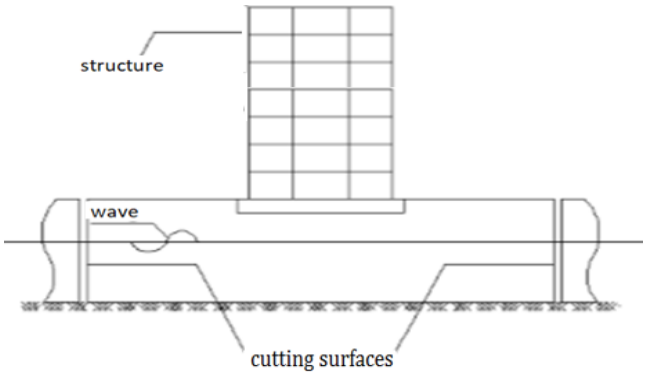

Fig. 1. Cutting soil surfaces (Guiterrez and Chopra 1978).

2.1.1. Features of the building models

As a numerical application, the influence of soil types on the nonlinear seismic behavior of a 7-storey frame system was investigated as shown in Figs. 2–3 and Table 1. The soil safety stress related to the material classes and behavior in the models used in the numerical application, for each of soil groups ZA, ZB, ZC, ZD and ZE specified in TBDY-2018 (2018), soil for each layer is divided into 30 layers depending on soil V_s velocity, soil group obtained with using the average of the mechanical properties calculated separately for each layer was used in modelling. In this section, the assumptions made about the building models and the features considered in the calculation of the models are as follows.

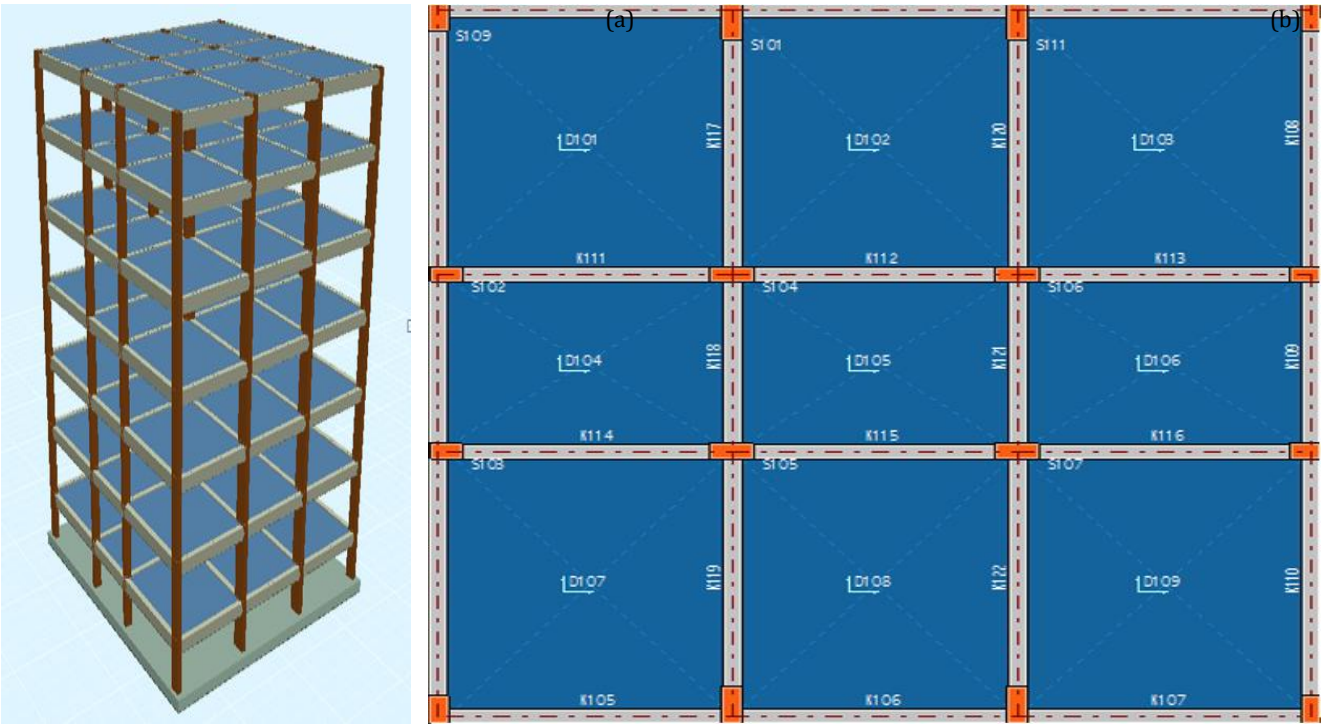

Fig. 2. (a) 3-D plan (b) of the 7-storey frame model.

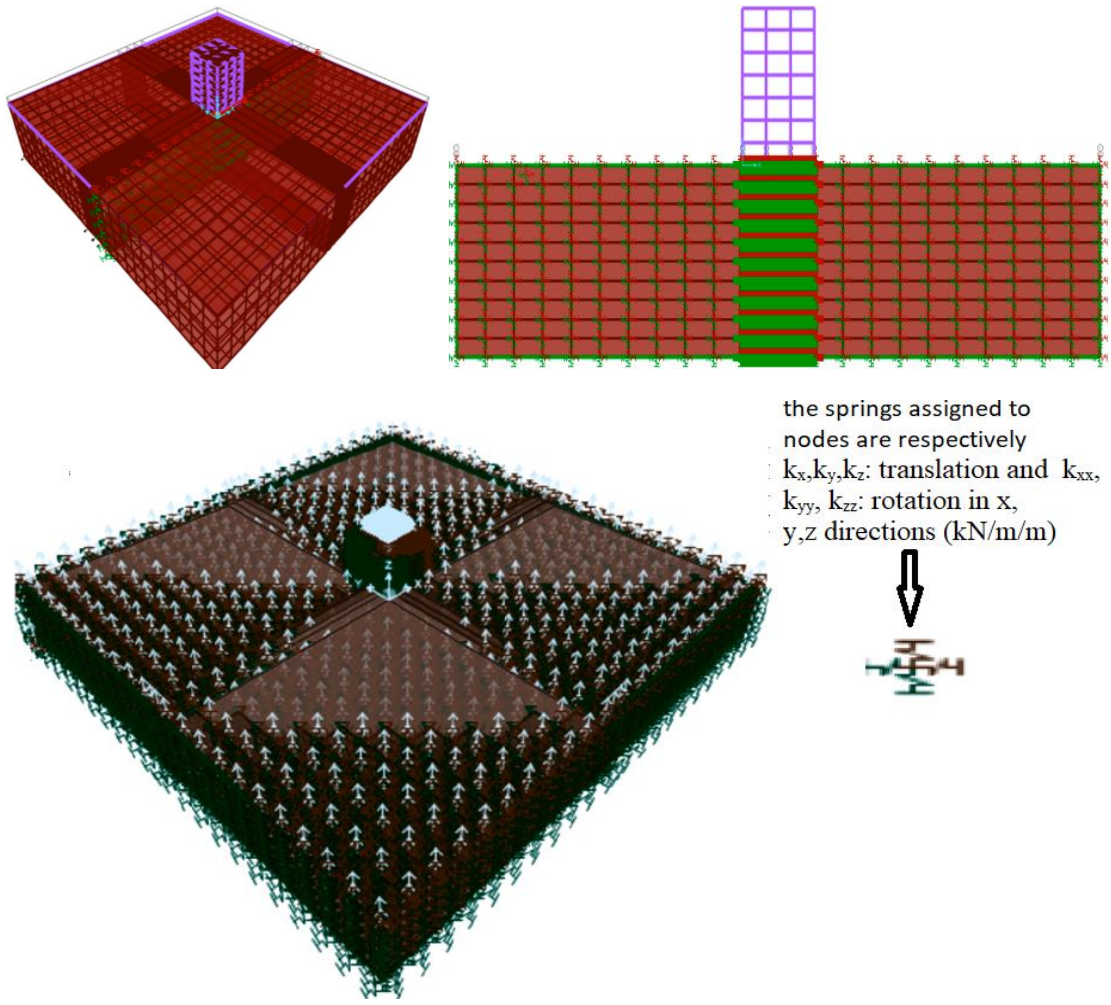

Fig. 3. 2D and 3D views of the 7-storey building.

Table 1. General characteristics of the building.

Number of floors	7
Purpose of usage	housing
Carrier system behavior coefficient	7
Building importance coefficient	1
Soil class	ZA, ZB, ZC, ZD, ZE
Base area	16.60·15.30=253.98 m²
Floor height	3
Total building height	45
Concrete class	C35
Steel class	S420
Live load factor (n)	0.3
Slab live load (t/m²)	0.2
Slab fixed load (t/m²)	0.3
External beam load (t/m²)	1.2
Internal beam load (t/m²)	0.8
Column dimensions	30×60, 30×80, 50×30, 70×30
Slab thickness	15 cm
Foundation thickness	60 cm

The depth of each soil is taken as 30 meters according to the TBDY-2018 (2018) Earthquake Code, and are divided into 30 layers, and the mechanical properties of the soil belonging to each layer are calculated with empirical formulas, assuming that V_s and V_p increase approximately linearly and equally in each interval.V_p, γ, E, G, parameters and q_n parameter showing the mechanical properties of the soils were calculated (Tezcan et al. 2006). Here, V_p and V_s are defined as longitudinal and transverse wave velocities (m/s), γ is defined as unit weight (kN/m³), E is defined as modulus of elasticity (kN/m²) and G is defined as slip modulus (kN/m²). μ is defined as Poisson's ratio and q_n is defined as soil safety stress (kg/cm²). The q_n parameter is taken as 30 meters for the depth of each soil according to the 2018 Earthquake Code, and the V_s and V_p wave velocities ranges are divided into 30 layers, and it is assumed that V_s and V_p increase linearly and equally in each interval, and the soil properties of each layer are calculated with empirical formulas calculated.

For calculations, the 7-floor lodging building, 135×135 dimensions and 30 meters deep, soil mass is taken into account, the lower part of soil is used as bedrock. Viscous boundaries (depending on effective stiffness and damping) are placed on the defined sides. Then, each soil group modeling was performed to represent the ZA, ZB, ZC, ZD and ZE soil groups specified in the

2018 Earthquake Code. Transverse wave velocity (V_s) ranges are specified in the ZA, ZB, ZC, ZD and ZE soil groups specified in the 2018 Earthquake regulations. In order to take into account the structure-soil interaction, the base dimensions of the 7-storey frame system building in the x, y, and z directions of the soil mass of 135×135×30 m, respectively, and the structure on this soil mass should be analyzed. According to the TBDY-2018 (2018) regulation, the earthquake was applied to the building in horizontal and vertical directions. After modeling both the building and soil, soil is divided into finite elements for ground interaction. Each finite element has 8 nodes and each node has 6 degrees of freedom in the x, y, z directions as translation and rotation (Gazetas 1991). Furthermore, In the Plastic Hinge Hypothesis, it is thought that the plastic deformations that are continuously spread in a region of length l_p on the rod element are collected at a point defined as the plastic hinge.

The spring constants were calculated for the 6 degrees of freedom to be assigned to the nodal points of the finite element belonging to the soil groups (Gazetas 1991).The spring constants are respectively k_x, k_y, k_z: translation in x, y, z directions (kN/m), k_{xx}, k_{yy}, k_{zz}: rotation in x, y, z directions (kN/m/m).In the definition of the dampers, the values obtained by using the equations defined in the literature for the horizontal and vertical components of the stiffness of the soil and the horizontal and vertical components of the damping ratio were used (Ala 2007). In the evaluation, it was assumed that the building model was on ZA, ZB, ZC, ZD and ZE class soils.

2.1.2. Earthquake acceleration recording features

Real earthquake records compatible with TBDY-2018 (2018) were selected to be used in dynamic analysis. The acceleration records required for nonlinear inelastic dynamic analyzes in the time history were selected using the PEER database (PEER, 2011). The station information, shear wave velocity ($V_{s,30}$) and scale coefficients of the selected acceleration record sets are given in Table 2.

Table 2. Selected earthquake records and their characteristics.

PEER no.	Earthquake	Year	Station	Earthquake magnitude	Shortest distance	Soil ($V_{s,30}$)
838	Landers	1992	Barstow	7.28	34.86	370
1101	Kobe Japan	1995	Amagazaki	6.90	11.34	256
1614	Düzce	1999	Lamont (1061)	7.10	11.46	481
1616	Düzce	1999	Lamont (362)	7.10	23.41	517
1619	Düzce	1999	Mudurnu	7.10	34.30	535
1636	Manjil	1999	Qazvin	7.37	49.97	303
1762	Hector Mine	1999	Amboy	7.13	41.81	383
3753	Landers	1992	Fun Valley	7.28	25.02	388
3757	Landers	1992	North P. Springs	7.28	26.95	367
5836	El Mayor	2010	Meloland G. Array	7.20	29.00	265
6969	Darfield	2010	Styx Mill Trans. St.	7.00	20.86	247

3. Analysis Results

In this study, the influences of soil types on non-linear seismic performance of reinforced concrete structures were investigated. In this context, the 7-storey frame system was modeled together according to ZA, ZB, ZC, ZD and ZE soil types according to TBDY-2018 (2018) and scaled with the SeismoSelect package program according to the simple scaling rule with real earthquake records. Analyzes were made. In the analyzes made, the building and soil were modeled together, and change of building base shear forces (tons), the number of structural elements with plastic hinge formed in the buildings, the max roof displacement (cm), the max inter-story drift ratio and the building soil periods (sec) and soil dominant periods were determined according to soil types has been investigated. Results are given in Tables 3–6.

4. Conclusions

In this study, it is investigated the influence of soil types on the nonlinear seismic behavior of reinforced concrete structures. For this purpose, 7-storey building models with different plans and rigidities were created. The behavior of these models under 11 different earthquake loads for the ZA, ZB, ZC, ZD, ZE soil types specified in the Turkish Building Earthquake Code has been examined. Analyzes were made using the time history method with the help of the SAP2000 program. According to analysis consequences, influence of soil types on the nonlinear seismic behavior of reinforced concrete structures is evaluated as below.

- The properties of the soil on which the building will sit are very important in terms of the non-linear earthquake behavior of the buildings. Because these properties of the soil are transmitted to the structures

by changing the magnitude of the earthquake acceleration and they are generally transmitted to the structures by increasing the magnitude of the earthquake acceleration from the ZA group soil to the ZE group soil. This situation is very important in terms of the magnitude of non-linear earthquake behavior in buildings.

- In the analyses, it is observed that the max peak displacement of building increases as elastic modulus of soil that is, stiffness of soil, decreases from ZA to ZE soil group. These values in the *x* and *y* directions 4.41-4.80 cm, 4.91-5.40 cm, 6.38-7.02 cm, 8.91-10.47 cm, and 12.6-13.81 cm, respectively.
- In the analyses, made with the 7-storey buildings, it was observed that the number of structural elements with plastic hinge increase as the elasticity modulus of the soils decrease from ZA to ZE soil group. While these values in a 7-storey building are from ZA soil group to ZE soil group, 74, 82, 117, 135, and 163 respectively.
- In the analyses, it is seen that the motion of soil and the amplitude of the earthquake vary depending on the soil properties, especially from ZA soil group to ZE soil group, due to the structure-soil interaction. This situation increases the cross-section influences that will occur in building, and accordingly, it has been observed that the level of non-linear behavior has increased.
- The variation of the effects of structural irregularities on the nonlinear seismic behavior of buildings according to soil types can be examined with different building models. In addition, the effect of concrete quality on the nonlinear seismic behavior of buildings according to soil types can be examined with different building models.

Table 3. 7-storey building base shear forces (tons).

Soil type	2018 TBDY	
	Direction	
	x	y
ZA	121.10	135.17
ZB	107.77	121.10
ZC	148.55	163.25
ZD	157.37	174.86
ZE	162.31	180.35

Table 4. Maximum peak displacement (cm).

Soil type	2018 TBDY	
	Direction	
	x	y
ZA	0.0055	0.0051
ZB	0.0066	0.0064
ZC	0.0093	0.0090
ZD	0.0127	0.0123
ZE	0.0155	0.0145

Table 5. Building periods (sec).

Soil type	2018 TBDY	
	Direction	
	x	y
ZA	0.73	0.68
ZB	0.83	0.77
ZC	1.11	1.04
ZD	1.57	1.47
ZE	2.28	2.12

Table 6. Soil dominant periods (sec).

Soil type	Soil dominant periods $t_o = 4H/V_s$ (s) (Keçeli 1990)	Building dominant periods $T=C_t \cdot HN_{0.75}$, C_t=0.1 (TBDY-2018 4.7.3.4(a) Eq. 4.27)
ZA	0.077	
ZB	0.107	
ZC	0.211	1.1
ZD	0.447	
ZE	0.720	

Acknowledgements

None declared.

Funding

The authors received no financial support for the research, authorship, and/or publication of this manuscript.

Conflict of Interest

The authors declared no potential conflicts of interest with respect to the research, authorship, and/or publication of this manuscript.

Author Contributions

All of the authors made substantial contributions to conception and design, or acquisition of data, or analysis and interpretation of data; were involved in drafting the manuscript or revising it critically for important intellectual content; and gave final approval of the version to be published.

Data Availability

The datasets created and/or analyzed during the current study are not publicly available, but are available from the corresponding author upon reasonable request.

REFERENCES

Ala N (2007). Adapazarı Zemininde Yapılan Betonarme Yapılarda Zemin-Yapı Etkileşimi, *M.Sc. thesis*, Sakarya University, Sakarya, Türkiye. (in Turkish)

ASCE 7-10 (2010). Minimum Design Loads for Buildings and Other Structures. ASCE Standard, ASCE/SEI 7-10. American Society of Civil Engineers, Reston, Virginia, USA.

Aviles J, and Perez-Rocha LE (1998). Effects of foundation embedment during building-soil interaction. *Earthquake Engineering and Structural Dynamics*, 27, 1523-1540.

Aydınoğlu MN (1977). Üstyapı-Zemin Ortak Sisteminin Deprem Hesabı. *Ph.D. thesis*, İstanbul Technical University, İstanbul, Türkiye. (in Turkish)

Aydınoğlu MN (1981). Yapı-Zemin Dinamik Etkileşiminin Genel formülasyonu ve Zemin Gömülü Yapılar için bir Alt Sistem Yöntemi. *Associate Professorship thesis*, İstanbul, Türkiye. (in Turkish)

Aydınoğlu MN (1994). Statik ve Dinamik Yapı-Zemin Etkileşimi., *Zemin Mekaniği ve Temel Mühendisliği 5. Ulusal Kongresi*, 218-229, METU, Ankara, Türkiye. (in Turkish)

Bettes P, Zienkiewicz OC (1969). Diffraction and refraction of surface waves using finite and infinite elements. *International Journal of Numerical Engineering*, 95(EM4), 859-877.

Bolisetti C, Whittaker AS, Coleman JL (2018). Linear and nonlinear soil-structure interaction analysis of buildings and safety-related nuclear structures. *Soil Dynamics and Earthquake Engineering*, 107, 218-233.

Castelli F. Grasso S, Lentini V, Sammito MSV (2021). Effects of soil-foundation-interaction on the seismic response of a cooling tower by 3D-FEM analysis. *Geosciences*, 11, 200.

Chian SC, Wilkinson SM, Whittle JK, Mulyani R, Alarcon JE, Pomonis A, Saito K, Fraser S, Goda K, Macabuag J, Offord M, Hunt-Raby AC, Sammonds P, Franco G, Stone H, Ahmed B, Hughes FE, Jirouskova NK, Kaminski S, Lopez J (2019). Lessons learnt from the 2009 Padang Indonesia, 2011 Tōhoku Japan and 2016 Muisne Ecuador Earthquakes. *Frontiers in Built Environment*, 5 (73), 1-20.

Eurocode-8 (2004). Design Provisions for Earthquake Resistance of Structures. European Committee for Standardization, Brussels.

Gazetas G (1991). Foundation Vibrations, Foundation Engineering Handbook. Van Nostrand Reinhold, 2nd edition, 553-593, New York, USA.

Gouasmia A, Djeghaba K (2007). Non-linear dynamic soil-structure interaction analysis of buildings. *Technological and Economic Development of Economy*, 13(4), 266-271.

Guiterrez JA, Chopra AK (1978). A substructure method for structures and geotechnical aspects. Earthquake *Engineering and Structure Dynamics*, 6, 51- 69.

Ichihara Y, Nakamura N, Moritani H, Choi B, Nishida A (2021). 3D FEM soil-structure interaction analysis for Kashiwazaki–Kariwa Nuclear Power Plant considering soil separation and sliding. *Frontiers in Built Environment*, 7, 676408.

Iida M (1998). Three-dimensional non-linear soil–building interaction analysis in the lakebed zone of Mexico city during the hypothetical Guerrero earthquake. Earthquake Engineering and Structural *Dynamics*, 27, 1483-1502.

Kayhan AH, Korkmaz KA, Irfanoglu A (2011). Selecting and scaling real ground motion records using harmony search algorithm. *Soil Dynamics and Earthquake Engineering*, 31, 941–953.

Lysmer J, Kuhlemeyer RL (1969). Finite dynamic model for infinite media, J*ournal of the Engineering Mechanics Division*, 95(EM4), 859-877.

Medina F (1980). Modelling of soil-structure interaction by finite and infinite elements. Report No. UCB/EERC-80/43, University of California, Berkeley, CA, USA.

Oz I, Senel SM, Palanci M, Kalkan A (2020). Effect of soil-structure interaction on the seismic response of existing low and mid-rise rc buildings. Applied Sciences, 10, 8357.

Parmelee RA (1967). Building-foundation interaction effects. *Journal of Engineering Mechanics Division*, 93(EM2), 131-152.

PEER Database (2011). University of California, Berkeley. http://nisee.berkeley.edu/spl/ [accessed 01-04-2023]

Pişen S, Pekşen E (2009). Sığ zeminler için farklı yöntemlerden elde edilen zemin emniyet gerilmesi değerlerinin karşılaştırılması. *Journal of Applied Earthsciences*, 8(2), 36-46. (in Turkish)

TBDY-2018 (2018). Türkiye Bina Deprem Yönetmeliği. Afet ve Acil Durum Başkanlığı, Ankara, Türkiye, 30364.

Tezcan SS, Ozdemir Z, Keceli A (2006). Allowable bearing capacity of shallow foundations based on shear wave velocity. *Journal of Geotechnical and Geological Engineering*, 24, 203-218.

Vicencio F, Alexander NA (2018). Dynamic interaction between adjacent buildings through nonlinear soil during earthquakes. *Soil Dynamics and Earthquake Engineering*, 10, 130-141.

Challenge Journal of Structural Mechanics

Research Article

Size effect on compressive behavior of GFRP bars

Meltem Eryilmaz Yildirim [a,*], Kerem Aybar [b], Mehmet Canbaz [a]

[a] *Department of Civil Engineering, Eskişehir Osmangazi University, 26480 Eskişehir, Türkiye*

[b] *Department of Metallurgical and Materials Engineering, Eskişehir Osmangazi University, 26480 Eskişehir, Türkiye*

ABSTRACT

In the last three decades, studies investigating the use of Glass Fiber Reinforced Polymer (GFRP) bars as an alternative to conventional steel rebars have increased due to their corrosive resistance. In addition to corrosion resistance, GFRP bars utilize high specific tensile strength, which makes them highly desirable in civil engineering applications. However, major design guidelines for GFRP-reinforced concrete structures currently do not consider their compressive contribution. Nevertheless, there is a growing trend in utilizing GFRP bars as compressive elements, driven by various studies demonstrating their ability to bear compressive loads effectively. This increasing demand underscores the need to comprehend the mechanical properties of GFRP bars, particularly in terms of their compressive behavior. Furthermore, a standardized test method to evaluate their compressive properties has not yet been developed. Addressing these gaps, this research paper focuses on investigating the influence of specimen size on the compressive strength of GFRP bars, specifically emphasizing on the compressive properties of GFRP bars. Compressive tests were conducted on GFRP specimens with varying diameters while maintaining a constant slenderness ratio. The findings from these compression tests shed light on the critical role of size in the compressive behavior of GFRP. This research emphasizes the importance of considering size as a significant parameter in designing mechanical properties for GFRP reinforcements.

ARTICLE INFO

Article history:
Received 25 July 2023
Revised 23 September 2023
Accepted 14 October 2023

Keywords:
GFRP bars
Compressive strength
Compression test
Mechanical properties

1. Introduction

Fiber reinforced polymer (FRP) bars have been a compelling alternative to conventional steel rebars thanks to their non-corrosive and high specific tensile strength (Benmokrane et al. 1995; Nanni 1993). However, their implementation has been limited due to a primary consideration of their behavior under compression. FRP bars are composites made from fibers that are embedded in a polymeric resin matrix binder. They feature exceptional properties such as high tensile strength, non-corrosiveness, high chemical resistance, lightweight, and non-conductivity (Balendran et al. 2002; Micelli and Nanni 2001; Saadatmanesh and Ehsani 1991). On the other hand, due to these composites' anisotropic and non-homogeneous nature, their behavior under compression is different from tension and is controlled by microstructural configuration. Tensile behavior and bond properties of GFRP bars have been investigated by several researchers (Al-Salloum et al. 2013; D'Antino and Pisani 2023; Galati et al. 2004; Özkal et al. 2018; Wiater and Siwowski 2020). However, compressive load carrying capacity of FRP bars has been neglected by codes and guidelines due to insufficient research (Al-Najmi and Abed 2020). GFRP bars exhibit high tensile strength but lower compressive strength. As a result, research efforts are predominantly directed towards understanding the mechanical behavior of GFRP under tensile loading; thus, studies on compressive behavior of GFRP rebars are limited (Zhou et al. 2023).

FRP materials have different application areas and can be manufactured in different geometries. FRP laminates have various application areas from industry to

* *Corresponding author*. Tel.: +90-222-239-3750 ; E-mail address: meryilmaz@ogu.edu.tr (M. Eryilmaz Yildirim)
ISSN: 2149-8024 / DOI: https://doi.org/10.20528/cjsmec.2024.01.003

construction. Lagoudas and Saleh (1993) investigated loading and geometry effects on the compressive strength of fibrous composites. Schultheisz and Waas (1996) investigated compressive testing methods and the micromechanical theories in compressive failure for fibrous composites. Berbinau et al. (1999) studied various unidirectional failure parameters for carbon-FRP (CFRP) laminates subjected to compressive forces. Soutis et al. (2002) explored the impact of specimen gauge section dimensions (length × width) on the compressive behavior of carbon/epoxy composites, examining the size-related factors. González and LLorca (2007) examined the mechanical response of unidirectional polymer composites subjected to transverse compressive loading. Zhou et al. (2013) the mechanisms leading to compressive damage in GFRP composites when subjected to off-axis loading. The authors conducted both experimental and computational investigations to analyze the microscale damage phenomena in GFRP composites at various angles between the loading direction and the fiber orientation.

Kobayashi and Fujisaki (1995) conducted compressive tests on FRP reinforcement. The researchers embedded FRP bars within a concrete prism, leaving a small space in the core. The experimental outcomes indicated that the compressive strength of the GFRP bars amounted to 30-40% of their tensile strength. Deitz et al. (2003) studied GFRP rebars under compression to investigate their ultimate capacity and Young's modulus. The authors developed a test method that consists of two steel rods, designed to thread into the heads of the testing machine. The holes in the steel rods were designed a bit greater than the diameter of the GFRP bars which effected the determination of actual slenderness ratios. Test findings show that, the maximum compression strength for non-slender specimens (unbraced length < 110 mm, diameter 15 mm) was almost 50% of their ultimate tensile strength. Bruun (2014) tested 25M (25mm diameter) GFRP bars under direct compression to investigate the relationship between compressive strength and the curve representing unbraced length interaction. According to the findings, the author demonstrated that 25 mm diameter GFRP bars with an elasticity modulus of 60 GPa experience crushing under monotonic loads when unbraced lengths are less than 230 mm (with an l/d ratio of approximately 9.0). Conversely, when the lengths are extended beyond 230 mm (resulting in an l/d ratio exceeding 9.2), may lead to random transition failure or weaker buckling failure. Khan et al. (2015) conducted compression tests on ∅15 mm GFRP bars and ∅15.9 mm CFRP bars using a modified version of the testing procedure outlined in ASTM D695-10. The longitudinal fibers of both GFRP and CFRP bars separated under compression, resulting a failure. The test findings indicated that the compressive strengths of GFRP and CFRP bars were 35% and 6% of their respective tensile strengths. Thiyagarajan et al. (2018) tested Basalt Fiber Reinforced Polymer (BFRP) bars by placing the specimens axially between the loading plates of the testing machine. Test results revealed that compressive strength of the BFRP bars were 50% of their tensile strength.

AlAjarmeh et al. (2019) proposed a new testing approach for assessing and characterizing the compressive behavior of GFRP bars. The authors employed cementitious grout-filled hollow steel caps to confine the top and bottom ends of the GFRP bars. The test findings indicated that as the unbraced bar length increased, the ratio of compressive strength to tensile strength decreased, resulting in a shift in the failure mode from crushing to fiber buckling. Zhang and Deng (2019) examined the compressive behavior of GFRP bars under sustained stress conditions in both a simulated marine environment and an alkaline solution simulating concrete conditions. In all tests, specimens of 10 mm diameter GFRP bars with a free length of 25 mm were employed. For the compressive tests, the authors used steel tubes grouted with epoxy resin matrix as enclosures at the bottom and top of the bars to avoid early failure of the GFRP bars. Abed et al. (2020) conducted dynamic and quasi-static tests to investigate the compressive strength and failure modes of GFRP and BFRP specimens. AlNajmi and Abed (2020) conducted compression tests on GFRP and BFRP samples with various diameters using steel caps in the ends of the specimens to decrease the effect of the samples tilting. The holes in the steel caps were also slightly bigger than the diameter of the specimen causing a decrease in the applied moment by the testing machine. Khorramian and Sadeghian (2021) suggested a test method for characterization of GFRP specimens under compressive forces, which includes rectangular steel plates, steel rings and anchorage adhesives. The unbraced specimen length is twice the diameter of the bars while the total length of the specimen is four times the diameter of the bars. The authors reported no buckling failure in the specimens. The failure modes included crushing in the unbraced length, crushing inside the casing and crushing of both in the unbraced length and in the casing. D'Antino and Pisani (2023) investigated tensile and compressive behavior of thermosetting and thermoplastic GFRP bars. The authors employed the compression test procedure given by Deitz et al. (2003).

Determining the compressive strength of composite bars is affected not only by the slenderness of the specimen but also by its size. This research investigates the influence of specimen size on the compressive strength of GFRP reinforcements. Compressive tests were conducted on specimens with varying diameters, while keeping the slenderness ratio constant. The obtained sigma-epsilon curves were analyzed to determine the compressive strengths, strain rates, toughness, and elastic moduli corresponding to each specimen size. This comprehensive analysis provides insights into the effect of specimen size on the mechanical properties of GFRP reinforcements under compression.

2. Experimental Study

The widespread usage of GFRP bars in structural elements guided the selection of reinforcement diameters. Recently, 10 mm diameter GFRP bars have increasingly been utilized as vertical reinforcements, commonly used

for shear reinforcement or stirrups. Additionally, 12 mm diameter GFRP bars are widely employed as longitudinal reinforcements in reinforced concrete beams. According to CSA S806-12 guidelines, GFRP bars with a diameter exceeding 15 mm are recommended for longitudinal reinforcement in columns. Consequently, to ensure representation of various scenarios, specimens with 10-, 12-, 18-, and 20-mm diameter GFRP bars were chosen for this study. The physical properties of the GFRP bars used in the experimental study are provided in Table 1.

Table 1. Properties of GFRP.

Fiber type	Resin type	Fiber content		Density (g/cm^3)
		by weight (%)	by volume (%)	
E-Glass	Vinyl Epoxy	> 75	>65	>1.80

The GFRP specimens were selected to have a slenderness ratio of 1.5, meaning that their length was 1.5 times their cross-section diameter. The slenderness ratio recommended by ASTM D695-15 (2002), ranging from 11 to 16, was not chosen due to the potential increase in local and global buckling.

Moreover, due to the heterogeneous and anisotropic nature of glass fiber reinforcements, there is currently no universally accepted standard test method for determining compressive strength. For each experiment, a minimum of 3 specimens were tested and average value of the test results are given in the graphs. The dimensions and images of the specimens are provided in Fig. 1.

Fig. 1. Test specimens.

The compressive test was conducted using the Shimadzu AG-IS 250kN Universal testing machine, as shown in Fig. 2. The crosshead speed was set at 0.5 mm/min, and the strain rate was determined to be $5x10^{-4}$ (s^{-1}).

Fig. 2. Compression test apparatus and GFRP specimen.

3. Discussion

Fig. 3 shows the GFRP specimens after the compression tests. It is observed that the 10 mm diameter specimens, subjected to compressive force along the fibers, experienced fiber separation and loss of integrity. On the other hand, the other specimens maintained their integrity under the same effect, although parallel cracks were observed along the fibers. These cracks occurred in the binder resin phase and not leading to fiber detachment. Analysis of the fracture patterns in these specimens revealed a brittle fracture mode without significant plastic deformation.

The stress-strain graph drawn under the effect of the axial compression force applied in the fiber direction is given in Fig. 4. Upon examining Fig. 4, it is evident that as the specimen diameter increases, indicating a size effect, the strength increases while deformations decrease. However, when the specimen diameter reaches 20 mm, a decrease in strength and an increase in deformations

are observed. As the specimen diameter increases, the fiber content also increases. In an anisotropic material, the increase in fibers plays a significant role in enhancing the strength of materials against forces applied along the fibers. Nevertheless, when the fiber content increases excessively, it becomes challenging for the resin to bond homogeneously. This leads to an increase in defects in the reinforcement cross-sectional area and a decrease in form stability, resulting in a decrease in strength. Upon closer examination of the stress-strain curve, initially a behavior close to linear elasticity is observed. As the load increases, localized fractures occur within the fiber-resin interface, causing a decrease in material resistance. Nevertheless, it can be observed that the stress continues to increase as the load is transferred to other fibers.

Fig. 3. Specimen images after compression test.

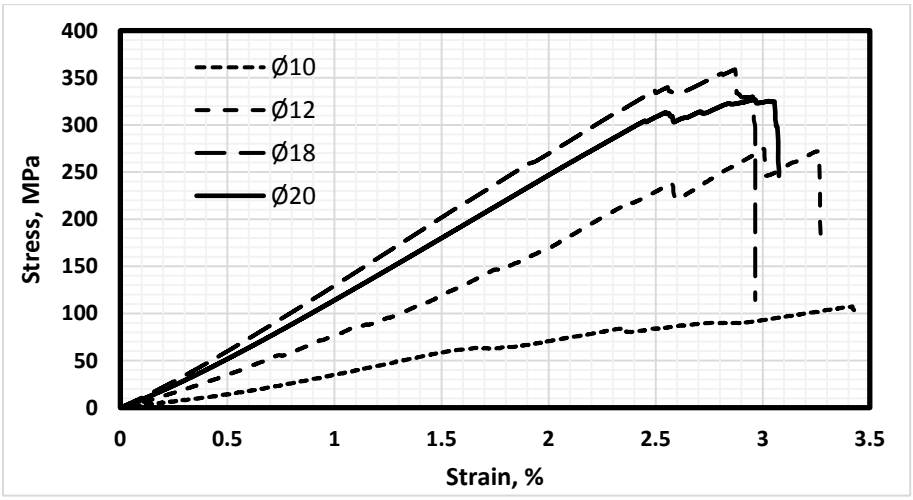

Fig. 4. Stress-strain graph of specimens under axial compressive force.

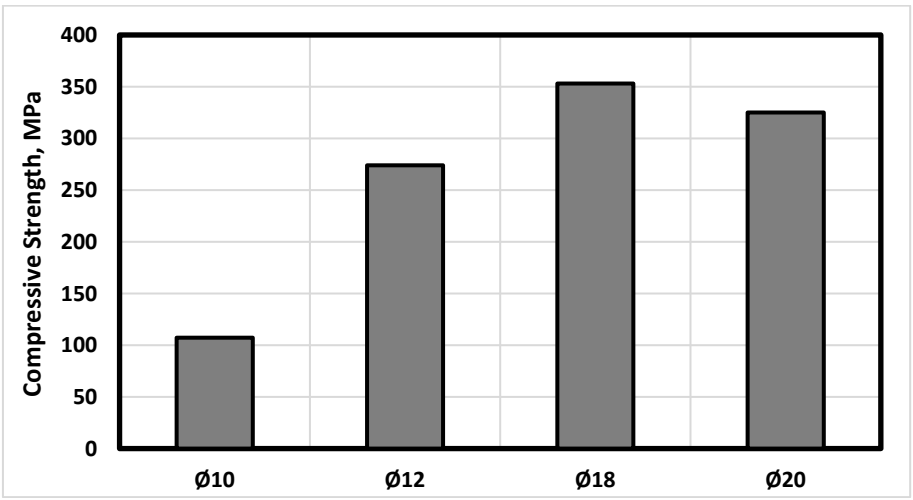

Fig. 5. Variation of compressive strength with size effect.

The variation of compressive strength in GFRP rebars concerning size effect is illustrated in Fig. 5. Experimental results show that the highest strength is observed in the 18 mm diameter GFRP specimen. As the diameter and fiber content decrease, a significant decrease in compressive strength is observed, reaching up to 70%.

However, when the diameter reaches 20 mm, the expected increase in compressive strength is not observed; instead, an approximate 8% decrease is observed between 18 mm and 20 mm diameter specimens. This decrease can be attributed to the increase in defects typically observed in brittle materials under the influence of size effect.

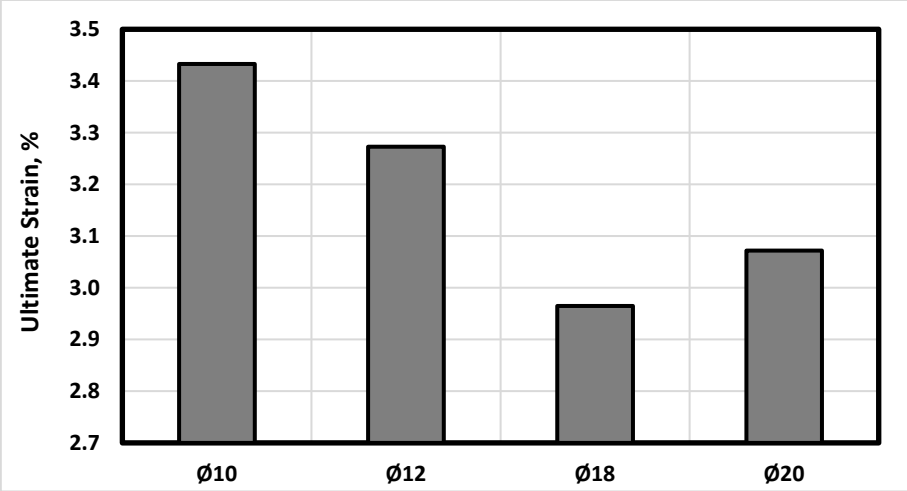

Fig. 6. Ultimate strain variation based on GFRP rebars diameter.

The size effect on the ultimate strain of GFRP rebars is given in Fig. 6. As the specimen diameter increases, along with an increase in fiber content, the resistance of the specimen to deformation increases. This leads to a decrease in strain ratios by approximately 13.6% when the diameter increases from 10 mm to 18 mm. Furthermore, when the specimen diameter reaches 20 mm, this decrease amounts to approximately 10.5%. The increase in specimen diameter results in an increase in defects originating from the binder resin, glass fiber, and their distribution. Consequently, it reduces the material strength of 20 mm specimen and leads to greater deformations compared to the 18 mm diameter specimen. These findings align with the changes observed in the compressive strength of the tested specimens.

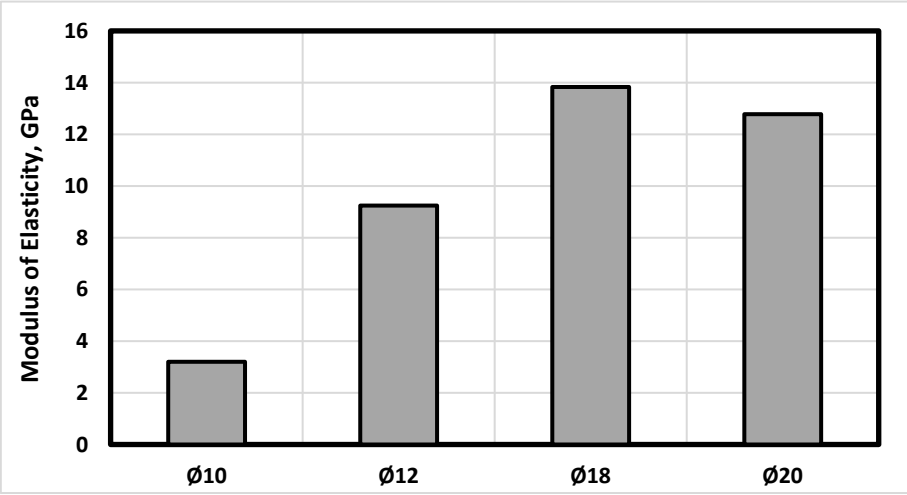

Fig. 7. Modulus of elasticity of GFRP specimens.

The relationship of the modulus of elasticity with the diameter in GFRP rebars is given in Fig. 7. The highest elastic modulus value is observed in the 18 mm diameter specimens, measuring 13.83 GPa. As the diameter decreases below 18 mm, a significant decrease of approximately 74% in the elastic modulus is observed, while an increase in diameter results in a decrease of approximately 7.6% for 20 mm specimen. The fibrous structure of GFRP, along with its anisotropic behavior and similarities to brittle materials, causes GFRP to undergo proportional deformation in response to stress until it reaches maximum stress, thereby influencing changes in elastic

moduli. The increase in binder resin content within the specimens hinders their deformation under the influence of external forces and enhances their rigidity, consequently elevating their elastic moduli. However, as previously mentioned, defects and voids become more prominent beyond the 18 mm diameter, facilitating deformation, and resulting in a decrease in the elastic modulus.

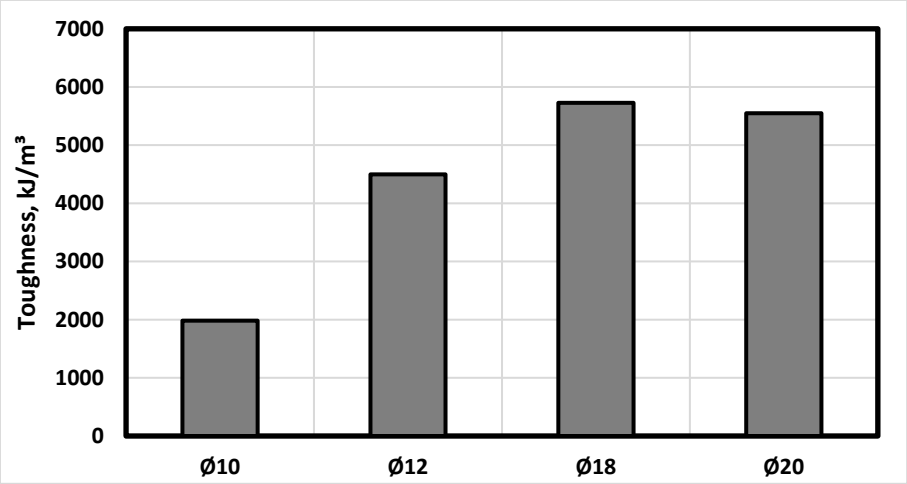

Fig. 8. Static toughness of GFRP rebars.

The static toughness values, calculated by considering the area below the stress-strain curve obtained from the compression tests on GFRP rebars, are presented in Fig. 8. It can be observed that the toughness value varies within the range of 1982-5727 kJ/mm^3. The toughness value increases by 2.26 times when the diameter increases from 10 mm to 12 mm, and it further increases by 2.88 times when it reaches 18 mm. However, when the diameter reaches 20 mm, the rate of increase decreases to 2.79 times. Based on these results, it can be concluded that in the size range up to 18 mm, the increase in fiber content and the lower amount of binder resin mitigates the effect of defects and contribute to an increase in toughness value. However, as the diameter exceeds 18 mm, the increased resin and fiber content gradually expose the influence of defects, resulting in a decrease in toughness values.

4. Conclusions

The following conclusions were reached as a result of the experimental study.

- It has been determined that under the effect of axial compressive forces, deformations and stresses increase proportionally until reaching the maximum value, and before the stresses reach their maximum, the brittle fractures in the glass fibers caused by longitudinal cracks between the fibers lead to a sudden decrease in stress. However, it has been observed that the stress continues to increase as the load is transferred to other fibers.
- The influence of size effect on the compressive strength of GFRP has indicated an increase in compressive strengths up to a diameter of 18 mm, exceeding 350 MPa, followed by a decrease beyond 18 mm.
- The study reveals that the deformation of GFRP specimens under axial compressive forces decreases as the specimen size increases. However, when the diameter exceeds 18 mm, the presence of defects becomes more prominent, leading to a decrease in the resistance to deformation.
- It has been observed that size effect is a significant factor affecting the modulus of elasticity in GFRP rebars, characterized by brittle and anisotropic fibers. Increasing the size results in an increase in the elastic modulus up to 13.8 GPa. However, beyond 18 mm, the presence of internal structural defects leads to a decrease in the elastic modulus, dropping down to 12.8 GPa.
- Size effect has been identified as an important parameter in the variation of toughness values of GFRP specimens. The highest toughness value of 0.00577 J/mm^3 was observed in the 18 mm diameter specimens.
- In structural engineering, while the size effect is not a significant factor influencing the strength of traditional steel rebars, which are isotropic, homogeneous, and ductile materials, under compressive forces, it has a detrimental effect on the strength of brittle, heterogeneous materials, especially due to internal structural defects that increase with size. GFRP, being a brittle and anisotropic material, exhibits high tensile strength but low compressive strength. In this study, it has been determined that the size of GFRP specimens affects not only the strength but also other mechanical properties under compressive forces. It is recommended to take the size effect into account when considering parameters related to mechanical properties in design. This study is primarily a preliminary work for the investigation of size effect. Conducting further experiments on different diameter size, and the other experimental and analytical studies in this area will improve the related standards, enabling the utilization of the GFRP bars for a wider application. Furthermore, it is suggested that the size effect be examined by increasing the specimen diameter at different slenderness ratios and supported by microstructure analysis for future studies.

Acknowledgements
None declared.

Funding
The authors received no financial support for the research, authorship, and/or publication of this manuscript.

Conflict of Interest
The authors declared no potential conflicts of interest with respect to the research, authorship, and/or publication of this manuscript.

Author Contributions
All of the authors made substantial contributions to conception and design, or acquisition of data, or analysis and interpretation of data; were involved in drafting the manuscript or revising it critically for important intellectual content; and gave final approval of the version to be published.

Data Availability
The datasets created and/or analyzed during the current study are not publicly available, but are available from the corresponding author upon reasonable request.

REFERENCES

Abed F, Mehaini Z, Oucif C, Abdul–Latif A, Baleh R (2020). Quasi-static and dynamic response of GFRP and BFRP bars under compression. *Composites Part C, Open Access* 2, 100034.

AlAjarmeh OS, Manalo AC, Benmokrane B, Vijay PV, Ferdous W, Mendis P (2019). Novel testing and characterization of GFRP bars in compression. *Construction and Building Materials,* 225, 1112–1126.

AlNajmi L, Abed F (2020). Evaluation of FRP bars under compression and their performance in RC columns. *Materials,* 13, 4541.

Al-Salloum YA, El-Gamal S, Almusallam TH, Alsayed SH, Aqel M (2013). Effect of harsh environmental conditions on the tensile properties of GFRP bars. *Composites Part B: Engineering,* 45, 835–844.

ASTM D695 (2015). Standard Test Method for Compressive Properties of Rigid Plastics. *ASTM International*. West Conshohocken, PA, USA.

Balendran RV, Rana TM, Maqsood T, Tang WC (2002). Application of FRP bars as reinforcement in civil engineering structures. *Structural Survey,* 20, 62–72.

Benmokrane B, Chaallal O, Masmoudi R (1995). Glass fibre reinforced plastic (GFRP) rebars for concrete structures. *Construction and Building Materials*, 353–364.

Berbinau P, Soutis C, Guz LA, Timoshenko LZP (1999). On the failure criteria for unidirectional carbon fibre composite materials under compression. *International Applied Mechanics,* 35, 462.

Bruun E (2014). GFRP bars in structural design: Determining the compressive strength versus unbraced length interaction curve. *Canadian Young Scientist Journal,* 2014, 22–29.

D'Antino T, Pisani MA (2023). Tensile and compressive behavior of thermoset and thermoplastic GFRP bars. *Construction and Building Materials,* 366, 130104.

Deitz DH, Harik IE, Gesund H (2003). Physical properties of glass fiber reinforced polymer rebars in compression. *Journal of Composites for Construction,* 7, 363–366.

Galati N, Vollintine B, Nanni A, Dharani LR, Aiello MA (2004). Thermal effects on bond between FRP rebars and concrete. *Advanced Polymer Composites for Structural Applications in Construction*, 501–508.

González C, LLorca J (2007). Mechanical behavior of unidirectional fiber-reinforced polymers under transverse compression: Microscopic mechanisms and modeling. *Composites Science and Technology,* 67, 2795–2806.

Khan QS, Sheikh MN, Hadi MNS (2015). Tension and compression testing of fibre reinforced polymer (FRP) bars. *The 12th International Symposium on Fiber Reinforced Polymers for Reinforced Concrete Structures (FRPRCS-12) & The 5th Asia-Pacific Conference on Fiber Reinforced Polymers in Structures* (*APFIS-2015*). Nanjing, China.

Khorramian K, Sadeghian P (2021). Material characterization of GFRP bars in compression using a new test method. *Journal of Testing and Evaluation,* 49, 20180873.

Kobayashi K, Fujisaki T (1995). Compressive behavior of FRP reinforcement in non-prestressed concrete members. *In: Taerwe L, editor. Non-metallic (FRP) Reinforcement for Concrete Structures,* 1st ed., Taylor & Francis Group, 267–274.

Lagoudas DC, Saleh AM (1993). Geometry and loading effects on the compressive strength of fibrous composites. *Journal of Reinforced Plastics and Composites,* 12, 1016–1023.

Micelli F, Nanni A (2001). Mechanical properties and durability of FRP rods. *CIES Report 00-22*. Rolla, MO: Taylor & Francis. http://www.crcnetbase.com/doi/10.1201/9780203883440.ch65.

Nanni A (1993). Fiber-reinforced-plastic (FRP) reinforcement for concrete structures. *Canadian Journal of Civil Engineering*, Elsevier.

Özkal FM, Polat M, Yağan M, Öztürk MO (2018). Mechanical properties and bond strength degradation of GFRP and steel rebars at elevated temperatures. *Construction and Building Materials,* 184, 45–57.

Saadatmanesh H, Ehsani MR (1991). Fiber composite bar for reinforced concrete construction. *Journal of Composite Materials*, 25, 188–203.

Schultheisz CR, Waas AM (1996). Compressive failure of composites, part I: Testing and micromechanical theories. *Progress in Aerospace Sciences,* 32(1), 1–42.

Soutis C, Lee J, Kong C (2002). Size effect on compressive strength of T300/924C carbon fibre-epoxy laminates. *Plastics, Rubber and Composites,* 31, 364–370.

Thiyagarajan P, Pavalan V, Sivagamasundari R (2018). Mechanical characterization of basalt fibre reinforced polymer bars for reinforced concrete structures. *International Journal of Applied Engineering Research,* 13, 5858–5862.

Wiater A, Siwowski T (2020). Comparison of tensile properties of glass fibre reinforced polymer rebars by testing according to various standards. *Materials,* 13, 4110.

Zhang X, Deng Z (2019). Durability of GFRP bars in the simulated marine environment and concrete environment under sustained compressive stress. *Construction and Building Materials,* 223, 299–309.

Zhou HW, Yi HY, Gui LL, Dai GM, Peng RD, Wang HW, Mishnaevsky L (2013). Compressive damage mechanism of GFRP composites under off-axis loading: Experimental and numerical investigations. *Composites Part B: Engineering,* 55, 119–127.

Zhou Z, Meng L, Zeng F, Guan S, Sun J, Tafsirojjaman T (2023). Experimental study and discrete analysis of compressive properties of glass fiber-reinforced polymer (GFRP) bars. *Polymers (Basel),* 15, 2651.

Challenge Journal of Structural Mechanics

Research Article

Structural behavior of historical Obruk Inn under different earthquakes

Süleyman Kamil Akın [a,*], Ahmet Alagöz [a]

[a] *Department of Civil Engineering, KTO Karatay University, 42020 Karatay, Konya, Türkiye*

ABSTRACT

Masonry structures is one of the most preferred structure types throughout history. The advantageous of these structures can be categorized as longevity, affordability and easy access to materials. Due to a lack of information and constructive errors, masonry structures suffer major damage under effect of earthquakes. While the vertical load carrying capacity of a masonry structure is excellent, its performance under horizontal loads is very poor. The brittle behavior of masonry structures, in particular, causes the structure to suffer significant damage or collapse completely during an earthquake. Türkiye is situated over a major earthquake zone. Throughout history, there has been numerous major earthquakes. These earthquakes have demolished the masonry structures resulted in significant life and economic losses. Therefore, in recent days, the examination of the seismic resilience performance of masonry structures as well as the required strengthening have become a pivotal issue. Thus, the aim of this study is to analyze the seismic performance of historical Obruk Inn subjected to different earthquake effects via finite elements method (FEM). To do this, the plans obtained from on-site inspections for historical Obruk Inn to create structural FEM model and its performance was evaluated under the influence of various earthquake excitations. As a result of the analyses, it was determined that the historical Obruk Inn structure should have immediate be strengthened against a possible earthquake.

ARTICLE INFO

Article history:
Received 19 December 2023
Revised 8 January 2024
Accepted 23 February 2024

Keywords:
Masonry structures
Finite element method
Earthquake performance
Historical structure

1. Introduction

Masonry structures are among the oldest types of structures that have been used throughout history (Kamal et al. 2014). As a result, the majority of masonry structures are historically significant but still in use (Gattesco et al. 2014). These structures have numerous advantages, including low cost, durability, and longevity (Hamid, 2006). Accordingly, the vast majority of building stock in Pakistan (93 percent), Mexico (76%), Peru (73%), and Italy (62%) is comprised of masonry building structures, including both existing and modern structures (Aşıkoğlu et al. 2020). The ability to pass through wide openings without columns, particularly thanks to the dome system, made it very popular in the construction of structures such as palaces and mosques during the Islamic period (Hejazi el al. 2015, and Hejazi et al. 2021). Therefore, Türkiye has a large number of historical masonry structures. Easy access to materials, particularly in rural areas, leads to greater preference. Moreover, masonry structures have many disadvantages as well as their advantages. While masonry structures can safely bear vertical loads thanks to rigid wall elements, their performance under horizontal dynamic loads, such as earthquakes, is poor (Pauletta et al. 2017). The complex structural configuration of masonry structures, as well as insufficient and incomplete knowledge of their structural systems, has a significant impact on the earthquake behavior of stacking structures (Asteris et al. 2014). Most countries have masonry structures that have manufacturing defects or have not received the required engineering service. These structures are exosed

* *Corresponding author*. Tel.: +90-444-1-251 ; E-mail address: kamil.akin@karatay.edu.tr (S. K. Akın)
ISSN: 2149-8024 / DOI: https://doi.org/10.20528/cjsmec.2024.01.004

to numerous horizontal load cycles during earthquakes causing great damage or collapse during a severe earthquake (Kollerathu et al. 2017). The poor earthquake performance of masonry structures, on the other hand, leads significant life and economic losses (Bruneau 1994; Tomazevic 1999). Hence not only in Türkiye, but also in all over the world the strengthening of masonry structures is required. One of the most important reasons for these amendments is the wear of the masonry structure due to time-dependent effects, the changing loading conditions due to unconscious modifications and changes in usage (Akcay et al. 2016). It is critical to determine the accurate seismic performance of masonry structures and to ensure the necessity of strengthening.

Anatolia is located on trade routes, many caravanserais were built, more specifically during the Anatolian Seljuk Period. Historical Obruk Inn Caravanserai is one of them. These structures, which were built at a distance of about 30-40 kilometers apart, were constructed to meet the needs of trade caravan groups. The Anatolian Seljuks used a plan scheme with closed and open courtyards to construct it. The historical Obruk Inn's entrance is to the west, and its facade is reminiscent of a castle, as shown in Fig. 1.

Fig. 1. Historical Obruk Inn.

It's located at the entrance to Obruk Village. It is right beside the Obruk Lake, which is also known as "Kızören Obruğu." (Fig. 2).

Faced stone, undressed stone and various spolia antique materials were used in its construction. The west facade, which houses the inn's entrance have two stories tall, while the other facades have single stories. Separate space arrangements were made on the second floor, and the masjid was also located here. Fig. 3 shows the building's ground, first and roof plans.

Modelling of structures and performing dynamic static analyses with the finite element method (FEM) is an extremely useful method for determining the causes of structural damage (Laefer et al. 2014; Tomaszewska 2010; Tomaszewska et al. 2012; Grillanda et al. 2019; Kujawa et al. 2020). Many studies are being conducted today to determine the earthquake behavior of masonry structures throughout FEM analysis (Asteris et al. 2014; Abruzzese et al. 2009; D'Agostino et al. 2009; Uzun et al. 2018; Sandoli et al. 2020, Theodossopoulos et al. 2013). In this study, the historical Obruk Inn's performance under the influence of different earthquake loads was investigated over SAP2000 structural analysis program.

At the present stage of knowledge, numerical simulations are fundamental to provide insight into the structural behavior and support the derivation of rational design rules but nonlinear finite element analyses will be always helpful for the validation of the design of complex masonry structures under complex loading conditions. In particular, computations beyond the limit load down to a possibly lower residual load are needed to assess the safety of the structure. Aside from failure analysis, also the serviceability limit states can be successfully validated with numerical analyses. FEM is a useful, reliable and valid tool for design and modelling of new and existing structures.

Another important aspect is the safety of existing structures under existing or new loading conditions, with an emphasis in the preservation of historical structures.

Reliable numerical models are necessary to assess and strengthen existing masonry structures. The final point is the need to improve the performance of masonry buildings in underdeveloped countries.

Fig. 2. Location of Historical Obruk Inn.

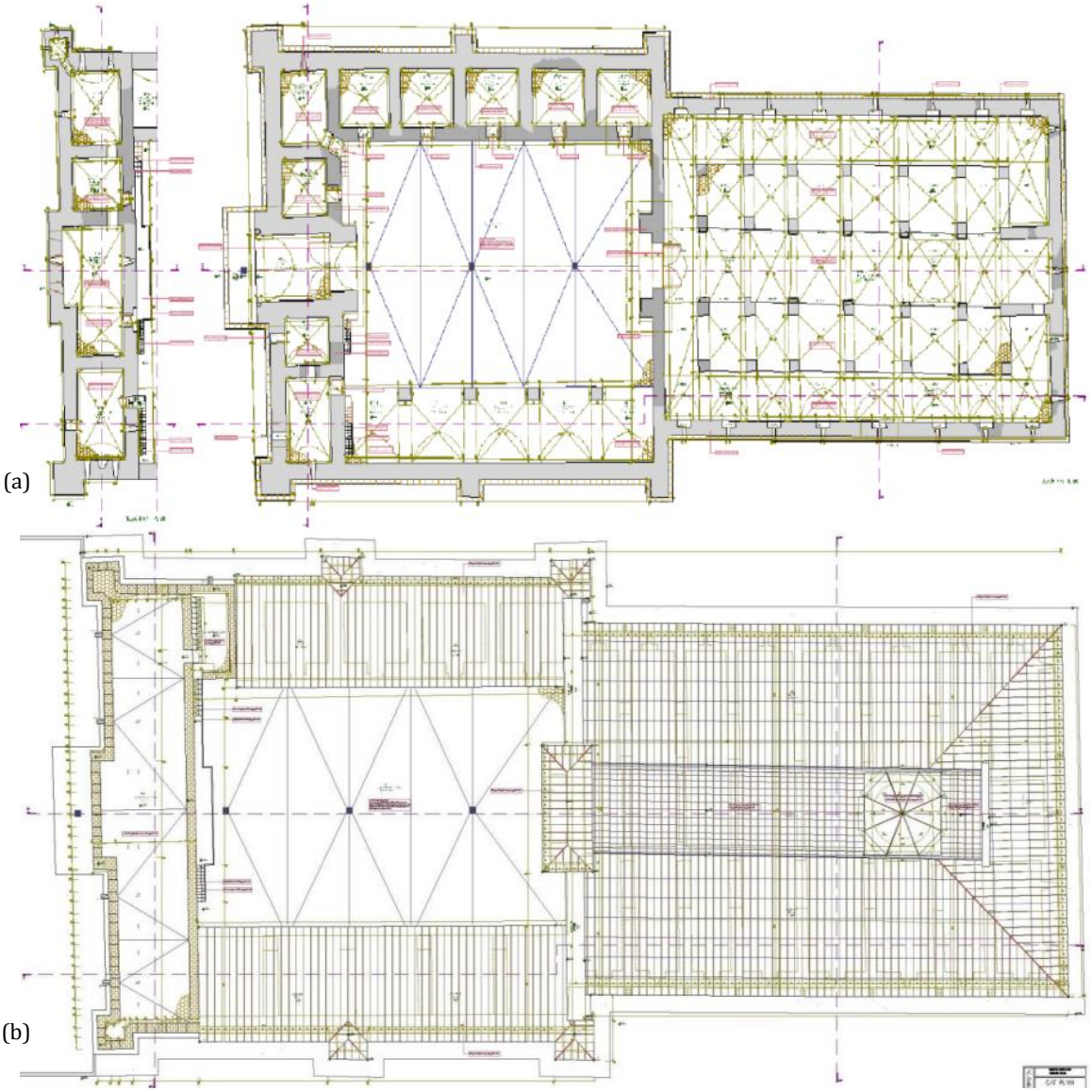

Fig. 3. Historical Obruk Inn: (a) Ground floor plan, (b) Roof floor plan.

2. Materials and method

2.1. Approaches to modeling of masonry structures

The modeling and evaluation of structures represent the most contentious issue among design engineers (Cakir 2022). Many studies had been made according to the modelling of unreinforced masonry structures. Evaluation of load carrying capacity of this type of structures usually needs to characterize the mechanical properties of the elements. For this reason, at first, the mechanical properties of constitutive materials including, bricks, adobes, mortars, pier elements of adobe and a vault element of brick were determined using standard experimental tests. Strength of a masonry building depends on both the bond between brick and mortar (Ahmadzai et al. 2022; Karaton and Çanakçı 2021). The results of samples tested, reconfirmed the very low tensile bond strength to be expected of masonry elements, emphasizing the inability of these types of materials to resist a tensile force. Finally, the mechanical properties of pier and vault testing samples were implemented in a nonlinear finite element (FE) analysis of the building, under lateral loading, through macro-modelling concepts (Eslami et al. 2012).

Masonry structures have a heterogeneous structural configuration made out of many dissimilar parts. These are wall material and mortar as binding material (Klinger 2010). Masonry structures typically have high weight, low tensile and shear strength, and behave brittle. The FEM is commonly used to perform numerical analyses for masonry structures. For this aim, firstly, the structure's finite element model should be created (Kamal et al. 2014). Vertical, horizontal, and rigid elements interactions between materials should be modelled correctly (Petrovčič et al. 2013). Additionally, the seismic behavior of masonry structures in general has been known for years. Geometry of structure, rigidity of horizontal and vertical elements to support the structure are the factors that affects the behavior of structure (Milani et al. 2017). For this reason, a number of modeling techniques are employed to reflect the behavior of the masonry construction. The Fig. 4 depicts these modeling techniques (Lourenço 1996).

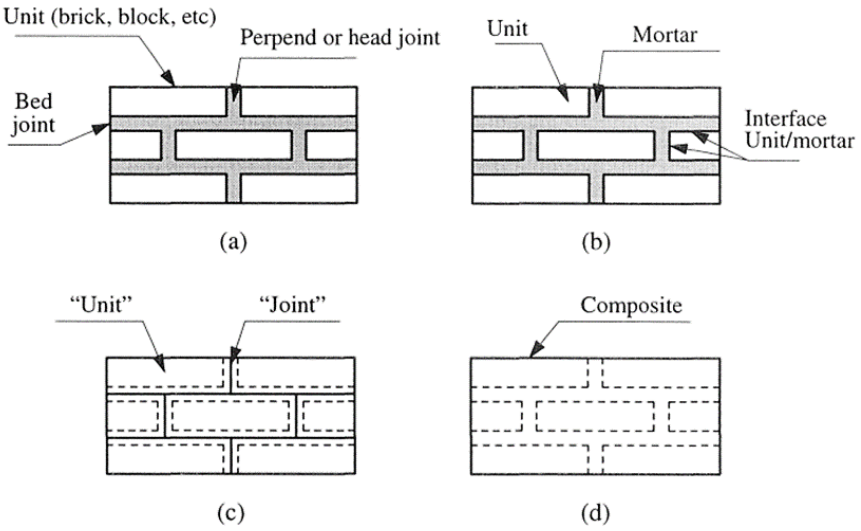

Fig. 4. Modelling methods for masonry structures: (a) Masonry sample; (b) Detailed micro-modeling; (c) Simplified micro-modeling; (d) Macro-modeling (Lourenço 1996).

2.1.1. Detailed micro modeling

In this case, masonry units and mortar joints are modeled as a continuum separately. In addition, as shown in Fig. 4a, a discontinuous interface is defined on the surface between the masonry units and the mortar joints. This type of modeling takes a lot of effort, but better results can be obtained. In scientific studies, this sort of modeling is widely preferred (Giordano et al.2017).

2.1.2. Simplified micro modeling

Without modeling the discontinuous interface between the mortar joint and the masonry structural unit, the bond between the mortar and the masonry structural unit is represented by continuous elements. This type of modeling is given in Fig. 4b.

2.1.3. Macro modeling

It is the simplest type of modeling. In this modeling technique, the mortar joints, masonry units, and unit/mortar interface are represented by continuum elements (Lourenço 1996). This type of modeling is given in Fig. 4c. This type of modeling is the most applicable modeling method. Especially in structures with long walls, a more uniform distribution of stresses is achieved (Chen et al. 2018).

2.2. Material properties

The building's structural system materials (inner and outer walls, as well as materials used in the vaults) were treated as two separate materials in the building model. The material properties mentioned in Table 1 are determined according to TEC-2007 (2007).

Table 1. Material properties.

Material	Modulus of elasticity (MPa)	Unit weight of bulk (kN/m^3)	Poisson's ratio
Mortar + stone	4500	24	0.20
Vaults	4000	18	0.18

2.3. Establishing the building model

In accordance with the actual building dimensions, the historical Obruk Inn was modeled in the SAP2000 structural analysis program. For modeling, the material properties listed in Table 1 were used. The building's walls are modeled as shell elements. The building's columns are modeled as rod elements. For stone and mortar, a homogeneous single material property was used for considering the macro modeling method. Fig. 5 depicts the building's three-dimensional model.

In the numerical model created, G1 is defined as a dead load, G2 as additional load, and Q as live load (snow load). Earthquake loads were applied to the system in X and Y directions as equivalent earthquake loads. EXP and EYP are defined as positive earthquake loads as well as EXN and EYN are defined as negative earthquake loads. In accordance with the earthquake code TEC-2007 (2007), the 5% eccentric effect was taken into account. The soil class of the region is Z3 according to TEC-2007 (2007). The building is located in the 5th degree earthquake zone. The building importance factor (coefficient) (I) has been taken as 1, and the earthquake load reduction coefficient (R), has been taken as 2 in line with the value determined by the Earthquake Code for masonry structures (TEC-2007). G2 additional loads were computed separately, taking into account the filling material used in the building, and live loads were taken in accordance with the earthquake code. Because the height of the area where the building is located is around 1000 meters above sea level, the snow load was determined as 0.8 kN\m^2 according to TS 498. Since the roof covering in closed area will be a lead plate (3 mm), the coating load has also been taken into account in the calculations. According to the rule that the total effective mass of the building should not be less than 90% of the total mass of the building, it is seen that the mass participation ratios in the x, y and z directions of the building exceed 90% in the last mode (Table 2).

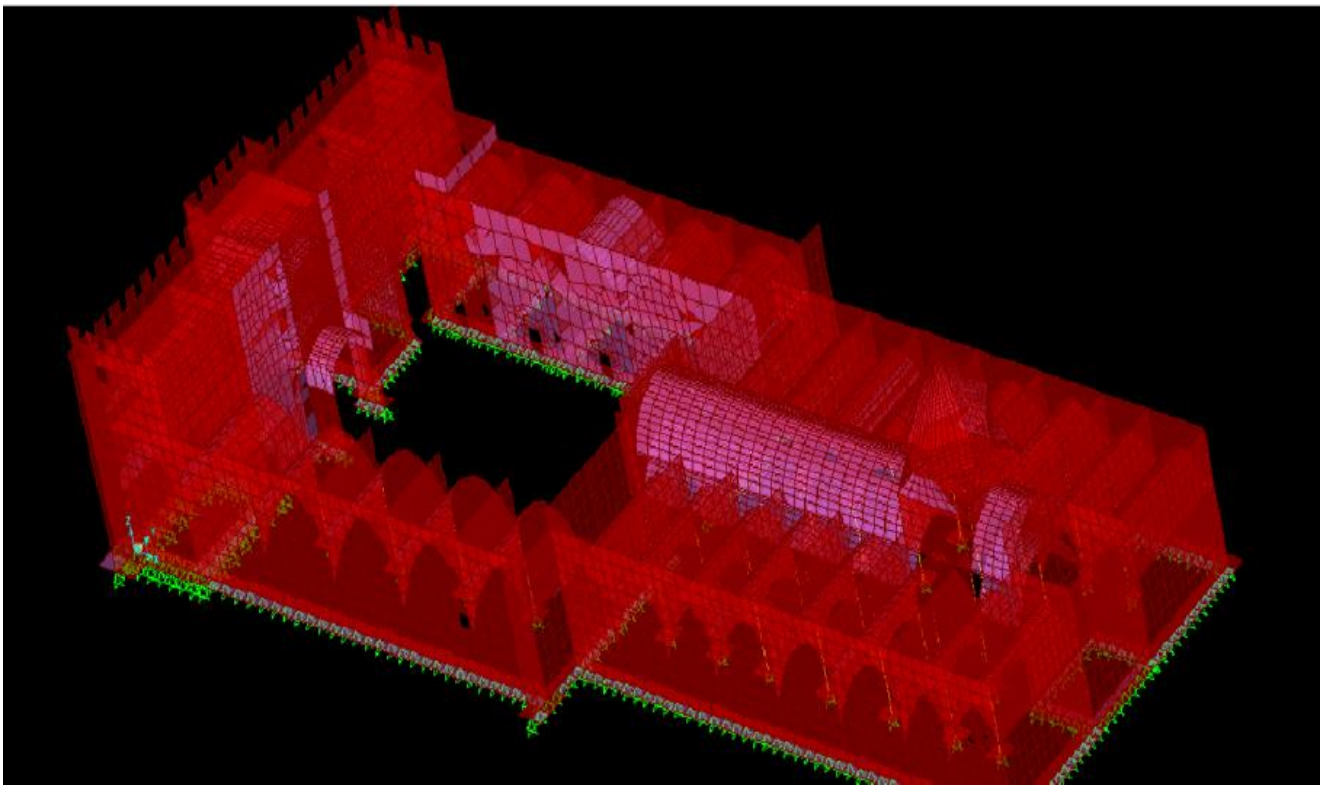

Fig. 5. Three-dimensional model of the structure.

The safe stresses for the materials were obtained by using the safety stress values for the materials with unknown unconfined compressive strength in the TEC-2007 (2007) code. The values defined in the code are listed in Table 3.

Table 2. Mass participation ratios and period.

Mode	Period (s)	Mass participation ratio UX (%)	Mass participation ratio UY (%)	Mass participation ratio UZ (%)
1	0.271344	0.00008104	0.05900	0.000004632
2	0.258326	0.00525	0.22931	0.00011
3	0.254005	0.20487	0.23524	0.00015
4	0.248451	0.20490	0.24469	0.00015
5	0.238386	0.21068	0.24471	0.00016
6	0.233619	0.21693	0.24576	0.00095
7	0.228081	0.21825	0.24882	0.00128
8	0.221302	0.22415	0.29566	0.00148
9	0.212641	0.23762	0.29639	0.00159
10	0.208915	0.26444	0.29639	0.00160
11	0.197601	0.27383	0.29668	0.00162
12	0.193502	0.27507	0.29668	0.00162
13	0.181558	0.27582	0.29671	0.00170
14	0.174658	0.28433	0.29673	0.00170
15	0.169962	0.28438	0.30109	0.00182
16	0.168491	0.28594	0.30609	0.00186
17	0.165680	0.35395	0.30650	0.00209
18	0.164603	0.38076	0.30656	0.00219
19	0.156734	0.38402	0.35651	0.00221
20	0.153036	0.38433	0.36416	0.00223
21	0.144948	0.38854	0.37368	0.00230
22	0.140602	0.39566	0.44897	0.00240
23	0.137722	0.54390	0.44940	0.00269
24	0.130412	0.55413	0.44997	0.00527
25	0.124780	0.55675	0.47982	0.00626
26	0.104597	0.55895	0.71655	0.00660
27	0.101820	0.56264	0.71684	0.01502
28	0.096905	0.56321	0.71735	0.05952
29	0.095192	0.56899	0.77423	0.06477
30	0.092200	0.58062	0.78328	0.08887
31	0.086529	0.66449	0.78522	0.09462
32	0.070033	0.66450	0.78647	0.17443
33	0.064365	0.66450	0.78647	0.21715
34	0.062405	0.66590	0.78650	0.33385
35	0.051892	0.67263	0.84691	0.33412
36	0.047345	0.68430	0.90480	0.33538
37	0.045430	0.90010	0.90509	0.33663
38	0.038496	0.90089	0.90629	0.55574
39	0.033089	0.90102	0.91253	0.57279
40	0.030616	0.90244	0.91484	0.90166

Table 3. Compressive safety stresses of walls with unknown unconfined compressive strength (TEC-2007).

Type of masonry unit used in the wall	Mortar wall pressure safety stress, f_{em} (MPa)
Vertically perforated block brick (with less than 35% cement-reinforced lime mortar)	1.0
Vertically perforated block brick (hole rate between 35-45%, with cement-reinforced lime mortar)	0.8
Vertically perforated block brick (with a cement-reinforced lime mortar with a hole rate of more than 45%)	0.5
Solid block brick or Blending brick (with cement-reinforced lime mortar)	0.8
Stone wall (with cement-reinforced lime mortar)	0.3
Aerated concrete (with adhesive)	0.6
Solid concrete briquette (with cement mortar)	0.8

The compression safety stress for stone masonry walls f_{em}=0.3 MPa and the compression safety stress for briquette masonry walls is f_{em}=0.8. On the other hand, the safety stresses are magnified by a factor of 3. In this case, the bearing stress for stone wall was assumed as $f_{em,b}$=0.3×3=0.9 MPa, and bearing stress for brick wall was assumed as $f_{em,b}$=0.8×3=2.4 MPa. Tensile stresses can be accepted as 15% of the value determined as compressive safety stress. In this case, the tensile safety stress for the stone wall was assumed as; $f_{em,ç}$=0.9×0.15=0.135 MPa and tensile stress for brick walls was assumed as; $f_{em,ç}$=2.4×0.15=0.36 MPa. The compressive and tensile stresses of the mentioned materials are given in Table 4.

Table 4. Acceptable safety stresses for materials.

Material	Compressive safety stress (MPa)	Tensile safety stress (MPa)
Brick (with mortar)	2.40	0.360
Stone wall (with mortar)	0.90	0.135

In order to apply the earthquake load effect to the structure, three different earthquake acceleration records were applied to the structure with the Time History Analysis Method. The characteristic features of the applied earthquakes are given in Table 5. The main reason to select those seismic records is that they have various effective magnitudes and different ground speeds as well as their seismic characterizations differ in regarded to ground accelerations and focal lengths. The earthquake acceleration records for each earthquake are given in Fig. 6.

Table 5. Characteristics of applied earthquakes.

Earthquake record	Date	Magnitude	Ground speed (cm/s)	Ground acceleration (g)	Focal length (km)	Type of earthquake
Kocaeli	08/17/99	7.51	58.85	0.312	13.60	Strike-slip
Landers	06/28/92	7.28	29.60	0.152	23.62	Strike-slip
Taiwan	08/21/99	6.20	14.63	0.132	12.44	Strike-slip

3. Results and Discussion

Analyses were run in the SAP2000 program using the parameters from the historical Obruk Inn. As a result, Fig. 7 depicts the distribution of maximum stresses under G+Q loading in the overall view of the structure. Tensile stresses exceeding the predicted tensile safety stress for the material were observed in the left part of the building's west facade as a result of the G+Q loading combination (Fig. 7a). Horizontal stresses on the front facade reach up to 0.540 MPa ($f_{em,ç}$=0.135 MPa) values. Although such high stresses are not seen intensively at the main entrance of the structure, they increase the expectation that crack-like deformations may occur in some

areas. Indeed, joint gaps and cracks have formed on the western front (Fig. 7b).

Base shear forces and displacements differ according to the geometry of the structure and acceleration. Different soil conditions should be studied also in further studies.

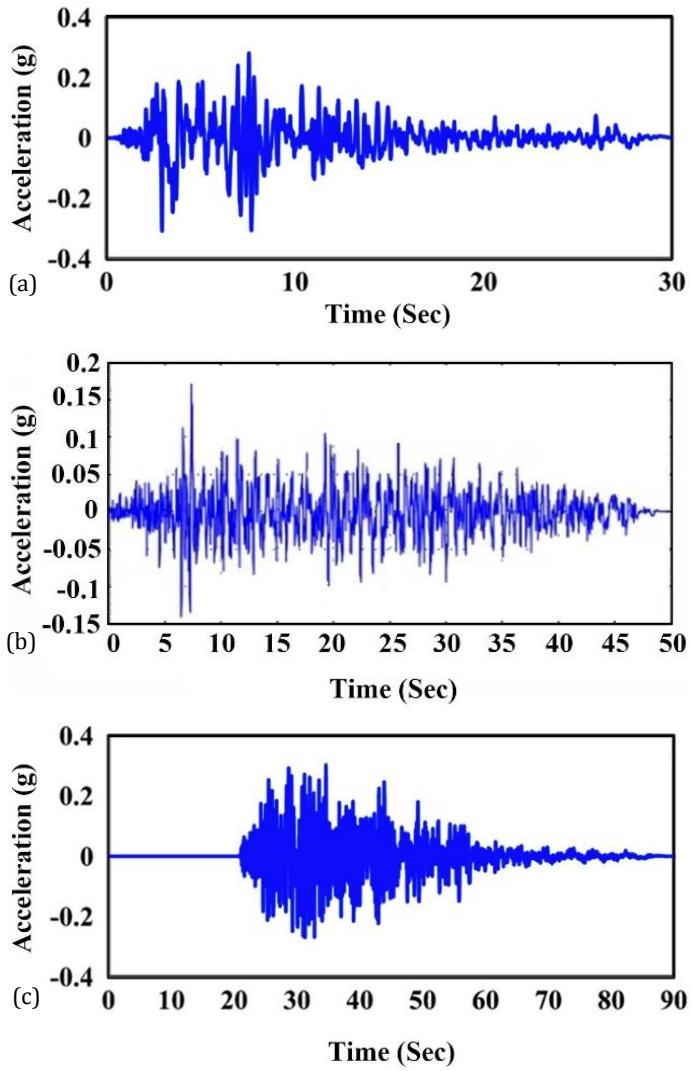

Fig. 6. Earthquake acceleration records: (a) Kocaeli; (b) Landers; (c) Taiwan.

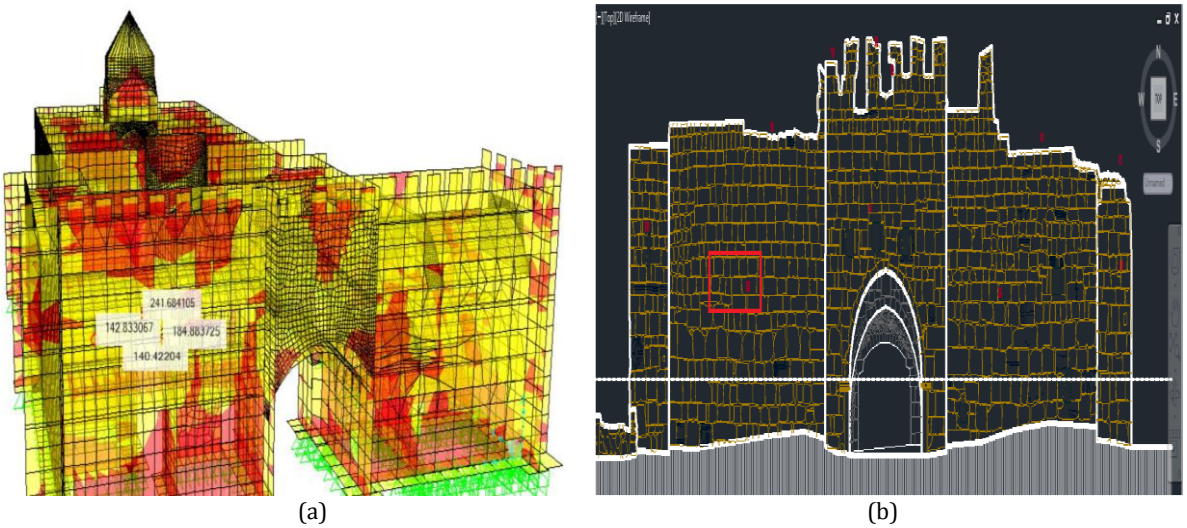

(a) (b)

Fig. 7. Historical Obruk Inn: (a) West facade maximum stress distribution under vertical loads; (b) West facade laser scanning result.

The examination of the building's eastern facade, as shown in Fig. 8, revealed that the tensile stresses in the horizontal direction reached up to 0.368 MPa value. As the stress value exceeded the tensile safety stress predicted for the material, joint gaps and dilatations occurred as a result of cracks at the points shown in the laser scanning of this facade, as shown in Fig. 8b, and this problem was resolved with new materials.

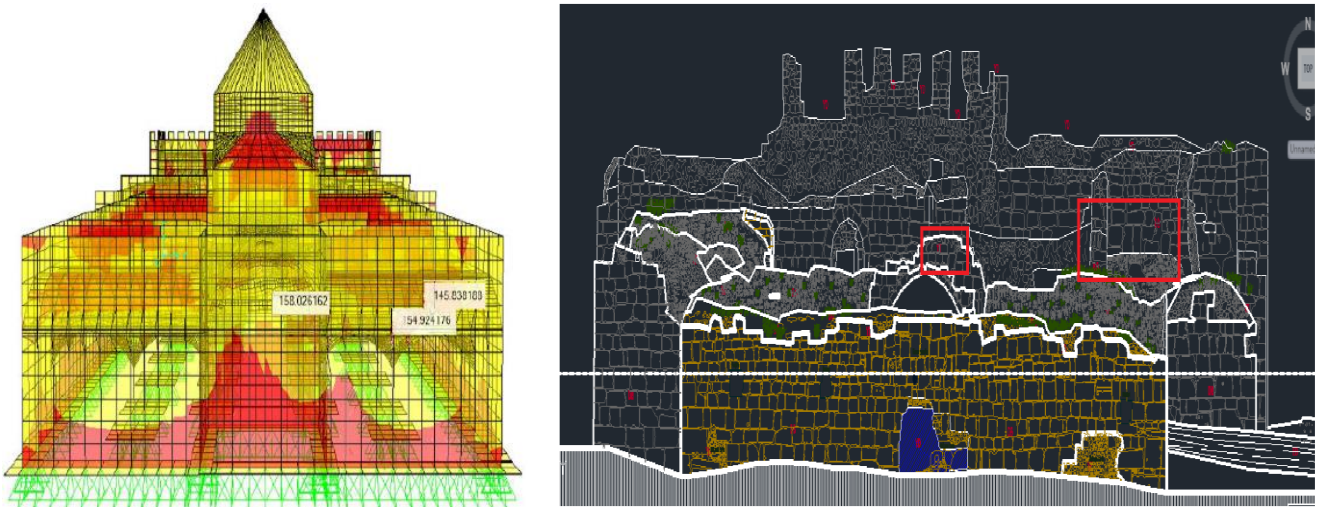

(a) (b)

Fig. 8. Historical Obruk Inn: (a) East facade maximum stress distribution under vertical loads; (b) East facade laser scanning result.

It was observed that the stresses in the open and closed volumes of the structure's south façade reached up to 0.463 MPa (Fig. 9a and Fig. 9c). These stresses are increasing in particular along the line where the vault arches of the structure connected to the outer wall. These stresses resulted in dilatations as a result of cracks in the middle section of façade which was repaired with new materials (Fig. 9b). The shape of the southern façade of the building created by laser scanning prior to restoration demonstrated the damage caused to the structure by the stresses that occurred in these areas (Fig. 9d).

The points up to 207.09 kNm^2 were detected in the closed volume of the building's northern façade (Fig. 10a), and these stresses caused small cracks in the middle of this façade, which were attempted to be repaired (Fig. 10b).

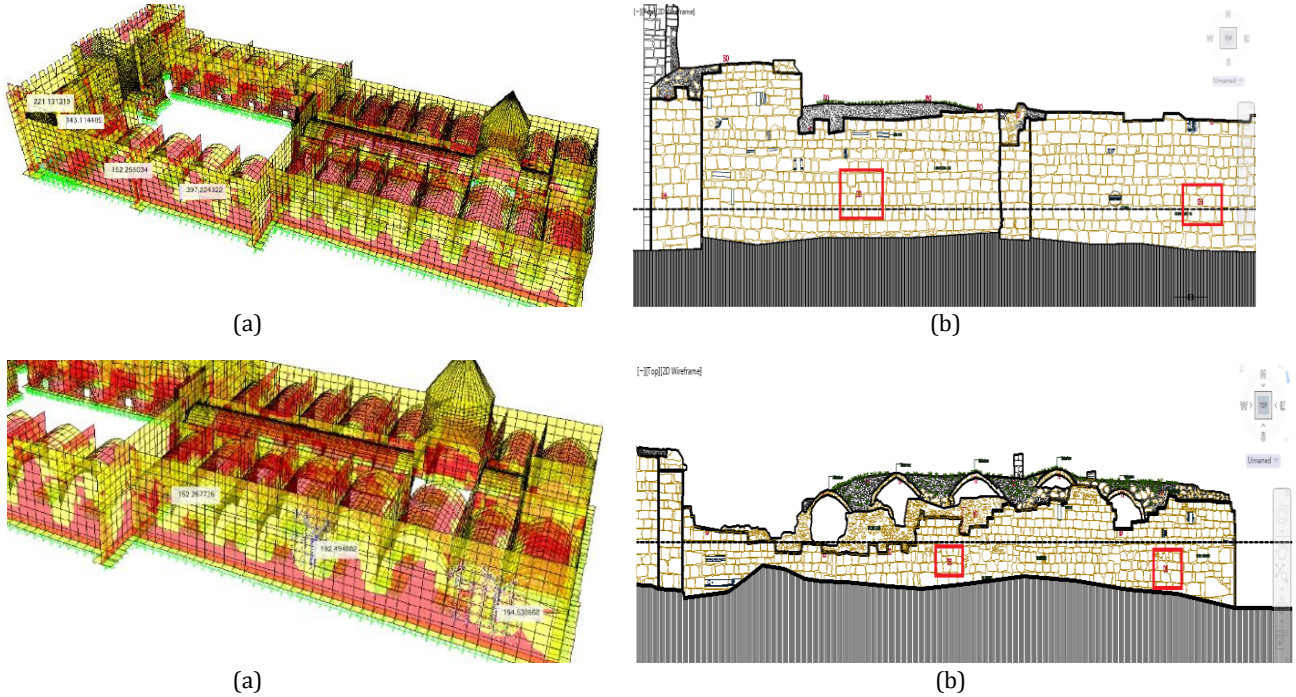

(a) (b)

(a) (b)

Fig. 9. Historical Obruk Inn: (a) South facade maximum stress distribution under vertical loads; (b) South facade laser scanning result; (c) Outer facade closed volume maximum stress distribution under vertical loads; (d) South facade closed volume laser scanning result.

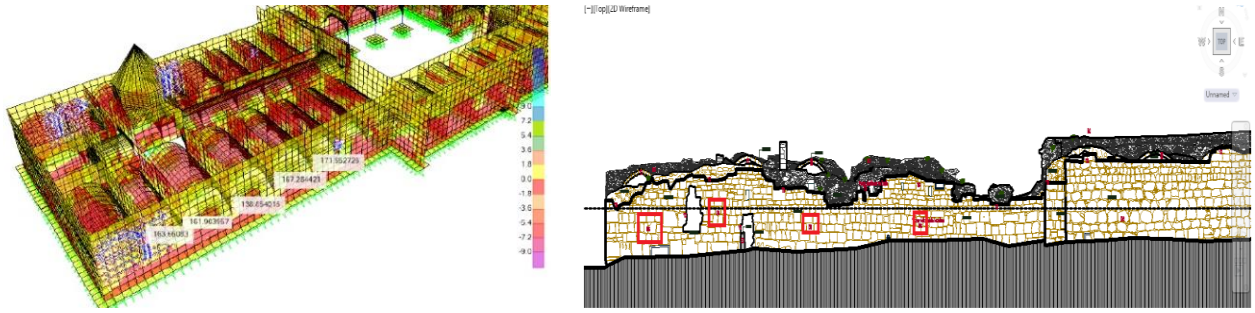

(a) (b)

Fig. 10. Historical Obruk Inn: (a) North facade maximum stress distribution under vertical loads; (b) North facade laser scanning result.

Base shear forces and displacements obtained by the time history analysis are given in Fig. 11. The compressive and tensile stresses occurred in the vaults as a result of the earthquake acceleration records applied are given in Fig. 12.

Under the influence of earthquakes, the vaults in the structure suffer significant strains. Individual stress distributions for each earthquake record are given in Fig. 13.

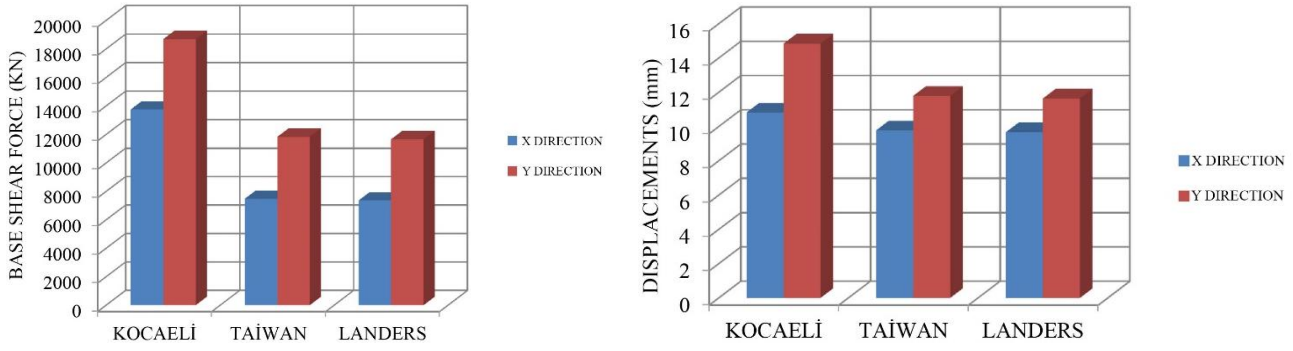

(a) (b)

Fig. 11. Time history analysis of historical Obruk Inn: (a) Base shear force; (b) Displacement.

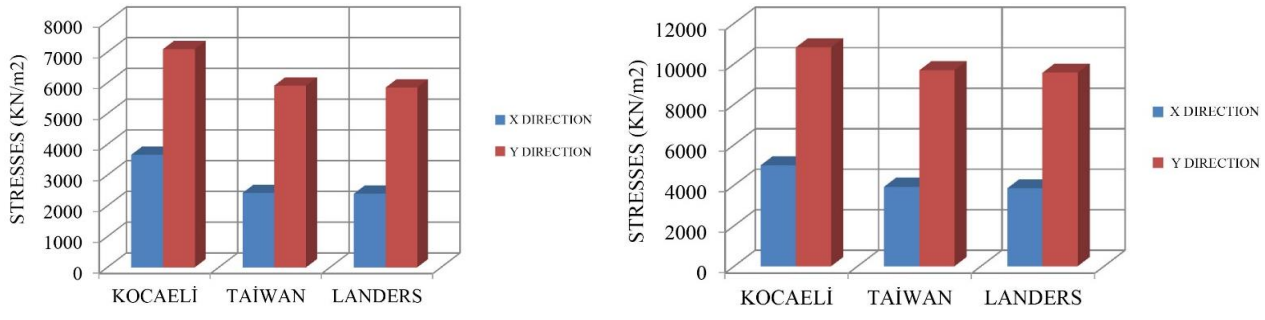

(a) (b)

Fig. 12. Time history analysis of historical Obruk Inn: (a) Tensile stresses in vault; (b) Compressive stresses in vault.

4. Conclusions

It is important to preserve historic buildings. The aim of this study is to understand the structural performance of historic masonry building. Obtained results of FEM analysis corrected the structural damage pattern of the existing building. The precautions should be taken immediately to preserve the building. Valid strengthening technics are being used for a long time.

Alhoubi et al. (2022) investigated the effectiveness of FRCM reinforcement in confining the columns and had Test results showed that confining the pre-damaged columns with PBO–FRCM systems resulted in 7–42% enhancement in their load-carrying capacity and 47–272% improvement in their ductility.

Tello et al. (2021) tested 12 short columns under axial compression, PBO-FRCM systems enhanced the capacity of columns. Columns strengthened with two and four PBO-FRCM layers showed a gain in the capacity of up to 40% and 75%, respectively.

Tello et al. (2023) had tested 4 rectangular and 4 circular columns under concentric loading. For each type of cross-section, columns were wrapped with 1, 2 or 4 layers of PBO FRCM. Overall, the strengthened columns exhibited higher load carrying capacity than their control unwrapped counterpart with an increase ranged between 5.1% and 36%.

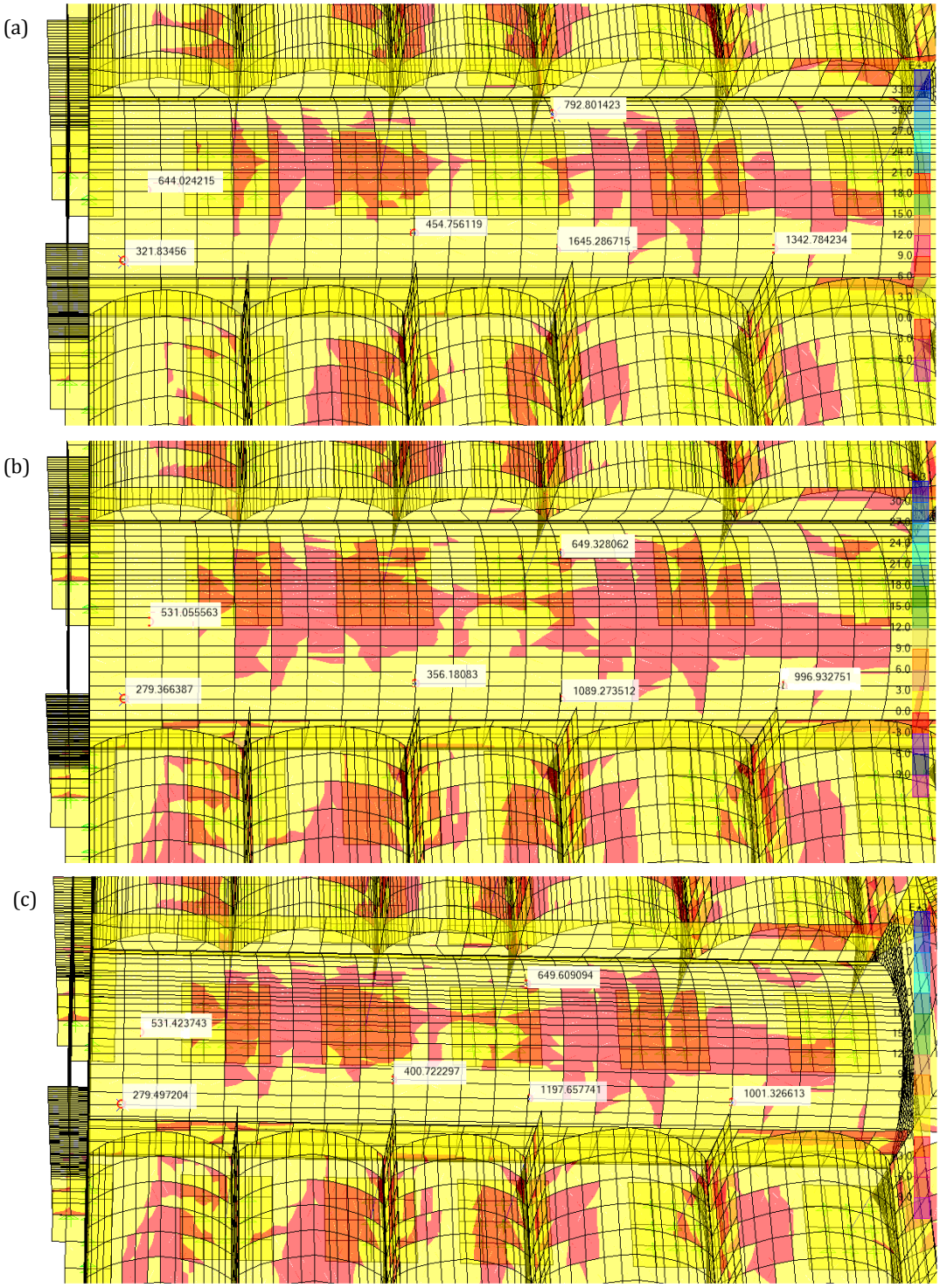

Fig. 13. Stresses in the vaults under the influence of earthquakes: (a) Kocaeli; (b) Lander; (c) Taiwan.

Kyaure and Abed (2021) studied a three-dimensional (3D) nonlinear finite element (FE) model and developed using ABAQUS to study the behavior of corrosion damaged RC columns retrofitted with poly-paraphenylene-ben-zobisoxazole (PBO) FRCM systems. Geometric and material nonlinearities in concrete, cement mortar and composite are incorporated in the FE model that is validated through axial capacity and failure mode comparisons against published literature.

The structural performance of the historical Obruk Inn under the influence of vertical and earthquake loads. was investigated in this work. The obtained results give ideas about the parts of the structure while strengthening. The following findings were obtained as a result of the study:

- High stresses exceeding the safety stress in the horizontal and vertical directions cause cracks in walls, vaults, arches, and other building elements, material losses, melting of materials, joint discharge, and many other problems.
- The highest strains in the structure were found at the vault and arches' supports, as well as at the upper

points of arches. While restoration newly strengthening methods should be used to preserve structural damages. Excessive deformation, particularly in the vault and arch parts of the structure, may result in sudden collapse.

- Analysis had showed that the stress and displacement values occurred by the Kocaeli earthquake records are greater than the maximum stress and displacement values occurred according to the Landers and Taiwan earthquake records. This is concluded because of the high base shear.
- The stress and displacement results from the Landers and Taiwan earthquake records are comparable.
- The structure should be strengthened immediately to prevent further damage from stresses caused by vertical loads.

Acknowledgements

None declared.

Funding

The authors received no financial support for the research, authorship, and/or publication of this manuscript.

Conflict of Interest

The authors declared no potential conflicts of interest with respect to the research, authorship, and/or publication of this manuscript.

Author Contributions

All of the authors made substantial contributions to conception and design, or acquisition of data, or analysis and interpretation of data; were involved in drafting the manuscript or revising it critically for important intellectual content; and gave final approval of the version to be published.

Data Availability

The datasets created and/or analyzed during the current study are not publicly available, but are available from the corresponding author upon reasonable request.

REFERENCES

Abruzzese D, Miccoli L, Yuan J (2009). Mechanical behavior of leaning masonry Huzhu Pagoda. *Journal of Cultural Heritage*, 10 (2009) 480–486.

Ahmadzai E, Yaman Z, Cumhur A (2022). Experimental examination of strength and behavior of masonry brick walls strengthened with expanded steel plates. *Challenge Journal of Structural Mechanics,* 8(3), 110-121.

Akcay C, Bozkurt TS, Sayin B, Yildizlar B (2016). Seismic retrofitting of the historical masonry structures using numerical approach. *Construction and Building Materials*, 113, 752–763.

Alhoubi Y, El Refai A, Abed F, El-Maaddawy T, Tello N (2022). Strengthening pre-damaged RC square columns with fabric-reinforced cementitious matrix (FRCM): Experimental investigation. *Composite Structures*, 294, 115784.

Asteris PG, Chronopoulos MP, Chrysostomou CZ, Varum H, Plevris V, Kyriakides N, Silva V (2015). Seismic vulnerability assessment of historical masonry structural systems. *Engineering Structures*, 62–63, 118–134.

Aşıkoğlu A, Vasconcelos G, Lourenço PB, Pantò B (2020). Pushover analysis of unreinforced irregular masonry buildings: Lessons from different modeling approaches. *Engineering Structures*, 218, 110830.

Bruneau M (1994). State-of-the-art report on seismic performance of unreinforced masonry buildings. *Journal of Structural Engineering*, 120.

Cakir F (2022). Performance-based assessment of long masonry structures. *Challenge Journal of Structural Mechanics*, 8(2), 47-56.

Chen SY, Moon FL, Yi T (2008). A macroelement for the nonlinear analysis of in-plane unreinforced masonry piers. *Engineering Structures*, 30, 2242–2252.

D'Agostino S, Lombardi G, Russo G, Viggiani C (2010). Structural engineering and geology applied to the static problems of the Etruscan "Tomba dell'Orco" (Tarquinia, Central Italy). *Journal of Cultural Heritage*, 11, 107–112.

Eslami A, Ronagh HR, Mahini SS, Morshed R (2012). Experimental investigation and nonlinear FE analysis of historical masonry buildings – A case study. *Construction and Building Materials*, 35, 251-260.

Gattesco N, Macorini L (2014). In-plane stiffening techniques with nail plates or CFRP strips for timber floors in historical masonry buildings. *Construction and Building Materials*, 58, 64–76.

Giordano A, Mele E, De Luca A (2002). Modelling of historical masonry structures: Comparison of different approaches through a case study. *Engineering Structures*, 24, 1057–1069.

Grillanda N, Chiozzi A, Bondi F, Tralli A, Manconi F, Stochino F, Cazzani A (2019). Numerical insights on the structural assessment of historical masonry stellar vaults: the case of Santa Maria del Monte in Cagliari. *Continuum Mechanics and Thermodynamics*, 1–24.

Hamid AA (2006). How to Face The Increasing Cost of Reinforcing Steel in RC Frame Construction in Egypt. Keynote Lecture, In: *Workshop of Proposed Alternatives to Face the Increasing Cost of Steel Reinforcement Used in RC Structures in Egypt*, Cairo, Egypt.

Hejazi M, Hejazi B, Hejazi S (2015). Evolution of Persian traditional architecture through the history. *Journal of Architecture and Urbanism*, 39, 188–206.

Hejazi M, Pourabedin M (2021). Performance of persian brick masonry discontinuous double-shell domes against earthquakes. *Engineering Failure Analysis*, 119, 104994.

Kamal OA, Hamdy GA, El-Salakawy TS (2014). Nonlinear analysis of historic and contemporary vaulted masonry assemblages. *HBRC Journal*, 10, 235–246.

Karaton M, Çanakçı K (2021). Yığma duvarların mikro modellemesinde harcın çekme dayanımı ve kayma gerilmesi iletim katsayısının çözümler üzerindeki etkisinin incelenmesi. *Dicle Üniversitesi Mühendislik Fakültesi Mühendislik Dergisi*, 12(1), 175-185. (in Turkish)

Klinger RE (2010). Masonry Structural Design. 1st ed., McGraw-Hill Professional.

Kollerathu JA, Menon A (2017). Role of diaphragm flexibility modelling in seismic analysis of existing masonry structures. *Structures*, 11, 22–39.

Kujawa M, Lubowiecka I, Szymczak C (2020). Finite element modelling of a historic church structure in the context of a masonry damage analysis. *Engineering Failure Analysis*, 107, 104233.

Kyaure M, Abed F (2021). Finite element parametric analysis of RC columns strengthened with FRCM. *Composite Structures*, 275, 114498.

Laefer DF, Truong-Hong L, Carr H, Singh M (2014). Crack detection limits in unit based masonry with terrestrial laser scanning. *NDT & E International*, 62, 66–76.

Lourenço PB (1996). Computational Strategies for Masonry Structures. *Ph.D. thesis*, Delft University, Delft, Netherlands.

Milani G, Shehu R, Valente M (2017). Possibilities and limitations of innovative retrofitting for masonry churches: Advanced computations on three case studies. *Construction and Building Materials*, 147, 239–263.

Pauletta M, Di Luca D, Russo E, Fumo C (2018). Seismic rehabilitation of cultural heritage masonry buildings with unbonded fiber reinforced elastomeric isolators (U-FREIs) – A case of study. *Journal of Cultural Heritage*, 32, 84–97.

Petrovčič S, Kilar V (2013). Seismic failure mode interaction for the equivalent frame modeling of unreinforced masonry structures. *Engineering Structures*, 54, 9–22.

Sandoli A, Musella C, Piero Lignola G, Calderoni B, Prota A (2020). Spandrel panels in masonry buildings: Effectiveness of the diagonal strut model within the equivalent frame model. *Structures*, 27, 879–893.

Tello N, Alhoubi Y, Abed F, El Refai A, El-Maaddawy T (2021). Circular and square columns strengthened with FRCM under concentric load. *Composite Structures*, 255, 113000.

Tello N, Farid A, El Refai A, El-Maaddawy T, Alhoubi Y (2023). Experimental investigation of pre-damaged circular RC columns strengthened with fabric-reinforced cementitious matrix (FRCM). *Structural Concrete*, 24, 1464-4177.

Theodossopoulos D, Sinha B (2013). A review of analytical methods in the current design processes and assessment of performance of masonry structures. *Construction and Building Materials*, 41, 990–1001.

Tomazevic M (1999). Earthquake-Resistant Design of Masonry Buildings. Imperial College Press.

Tomaszewska A (2010). Influence of statistical errors on damage detection based on structural flexibility and mode shape curvature. *Computers & Structures*, 88, 154–164.

Tomaszewska A, Szymczak C (2012). Identification of the Vistula Mounting tower model using measured modal data. *Engineering Structures*, 42, 342–348.

TEC-2007 (2007). Specifications for buildings to be built in seismic areas. Turkish Earthquake Code, Ankara, Türkiye.

TS-498 (1997). Design Loads for Buildings. Turkish Standard Institute, Ankara, Türkiye.

Uzun M, Korkmaz HH (2018). Investigation of numerical analysis according to two different methods of an existing masonry building, *Journal of Engineering Research and Applied Science*, 7, 965–971.